2019

Distributed Control of Electric Vehicle Charging: Privacy, Performance, and Processing Tradeoffs

Micah Botkin-Levy
University of Vermont

Distributed Control of Electric Vehicle Charging: Privacy, Performance, and Processing Tradeoffs

A Thesis Presented

by

Micah Botkin-Levy

to

The Faculty of the Graduate College

of

The University of Vermont

In Partial Fulfillment of the Requirements
for the Degree of Master of Science
Specializing in Electrical Engineering

May, 2019

Defense Date: March 25th, 2019
Dissertation Examination Committee:

Mads Almassalkhi, Ph.D., Advisor
James Bagrow, Ph.D., Chairperson
Paul Hines, Ph.D.
Cynthia J. Forehand, Ph.D., Dean of Graduate College

ABSTRACT

As global climate change concerns, technological advancements, and economic shifts increase the adoption of electric vehicles, it is vital to study how best to integrate these into our existing energy systems. Electric vehicles (EVs) are on track to quickly become a large factor in the energy grid. If left uncoordinated, the charging of EVs will become a burden on the grid by increasing peak demand and overloading transformers. However, with proper charging control strategies, the problems can be mitigated without the need for expensive capital investments. Distributed control methods are a powerful tool to coordinate the charging, but it will be important to assess the trade-offs between performance, information privacy, and computational speed between different control strategies.

This work presents a comprehensive comparison between four distributed control algorithms simulating two case studies constrained by dynamic transformer temperature and current limits. The transformer temperature dynamics are inherently nonlinear and this implementation is contrasted with a piece-wise linear convex relaxation. The more commonly distributed control methods of Dual Decomposition and Alternating Direction Method of Multipliers (ADMM) are compared against a relatively new algorithm, Augmented Lagrangian based Alternating Direction Inexact Newton (ALADIN), as well as against a low-information packetized energy management control scheme (PEM). These algorithms are implemented with a receding horizon in two distinct case studies: a local neighborhood scenario with EVs at each network node and a hub scenario where each node represents a collection of EVs. Finally, these simulation results are compared and analyzed to assess the methods' performance, privacy, and processing metrics for each case study as no algorithm is found to be optimal for all applications.

Acknowledgements

First, I would like to thank my advisor, Professor Mads R. Almassalkhi, for encouraging me to continue learning and his support, guidance, and insight throughout my work.

Next, I wish to thank Professor Paul Hines and Professor James Bagrow for their interest in my work and serving as members of my thesis committee.

My thanks also goes out to the researchers at the Karlsruhe Institute of Technology for letting me visit and share knowledge.

Finally, I would like to thank my family and friends for their love and support throughout the whole process.

TABLE OF CONTENTS

LIST OF TABLES

LIST OF FIGURES

CHAPTER 1

INTRODUCTION

1.1 MOTIVATION

Electric vehicles (EVs) have become a popular alternative to fossil-fuel based transportation and interest in electrifying the transportation sector will only continue to grow in the future. As we continue to utilize more renewable forms of energy as electricity sources, powering our transportation section on the electric grid instead of fossil fuels will reduce emissions and climate change impacts. Increasing levels of funding are being invested into R&D for efficient and low-cost lithium-ion batteries for EVs, which will continue to drive down costs [1, 2]. In addition, electric vehicles have been shown to be cheaper to maintain and operate as well as safer than the traditional options [3–5].

These economic and societal benefits have already spurned a growth in the production and sales of electric vehicles. For example, in California 1 in 10 new car purchases are electric vehicles [6]. In addition, there has been growing interest in electric non-residential vehicles such as metro area public transit, pickup trucks, semi-trailer

trucks, and other delivery vehicles. Not only have major car manufactures committed to electrifying a portion of their products in the coming years, but leading trucking and delivery companies have already been piloting electric vehicle fleets.

However, there are certain challenges associated with increased adoption of electric vehicles. Converting this traditionally fossil-fuel based energy demand to electricity will add demand to the electric grid and change the shape of the demand curve. Most residential users will charge their vehicles when they come home from work, which coincides with the evening peak in energy usage. This will only exacerbate the ramping caused by the increased penetration of solar PV, i.e., the so-called "Duck Curve" [7–9].

On a more local level, uncoordinated charging from electric vehicles can lead to demand that exceeds the rating of the nearby distribution substation power transformer. This MVA-scale oil-filled transformer has its cores immersed in mineral oil for improved heat transfer. Additional EVs will increase the demand on a transformer, which in turn increases the hot-spot temperature of the transformer, which is the hottest spot inside the transformer. The hot-spot temperature is a major factor in transformer wear-and-tear and aging as the hot oil will break down the winding insulation faster [10]. In order to accurately model the transformer hot-spot temperature dynamics, a high order, non-linear thermodynamic model, such as the IEEE Standard C57.91-1995 (e.g., *Clause 7* and *Annex G*) is usually used.

Thus, it is desirable to schedule EVs with respect to the hot-spot temperature constraint and EV-specific objectives, which form an optimization problem. Due to the potential for a high number of EVs and a large time horizon, this optimization problem is computationally challenging. Techniques such as decomposition are used

to separate the large scheduling problem with coupling constraints into smaller ones. Two more common algorithms used are dual decomposition with dual ascent and Alternating Direction Method of Multipliers (ADMM). Two uncommon distributed methods that will be discussed in this work are Augmented Lagrangian based Alternating Direction Inexact Newton (ALADIN), as well as a packetized energy management control scheme (PEM).

In order to assess which of these algorithms fit our applications needs the best, we will be evaluating them on three metrics. First, we will measure how well they perform when compared with the original central problem. Next, we will quantify how well the algorithms reduce the communication overhead and protect the information of the electric vehicle owners. Finally, we will use metrics to track the computational speed of the algorithms.

1.2 Literature Review

Recent years have seen a growth in papers that study the control of EV charging. General comparisons of non-centralized control techniques exist such as [11, 12]. There are papers that utilize dual decomposition to solve the EV charging control problem [13–15] as well as multiple papers which used an ADMM approach for some variation of the EV charging problem [16–21]. Other papers have novel or creative approaches such as [22] which explored EV charging for valley-filling under transformer constraints using shrunken-primal-dual subgradient (SPDS) algorithm, [23–25] which employ random charging requests, and [26–28] which uses game theory.

With the increase in interest in controlling electric vehicle charging comes a grow-

ing concern for protecting electric vehicle owner's information. Papers have begun to look at ways to coordinate the charging of electric vehicles while minimizing or eliminating the need to communicate information to a central coordinator. Many such as [29–31] use peer-to-peer or blockchain technologies to enable transactive energy trading.

Few papers that study the EV charging problem compare multiple algorithms. The work done in [21] computes the optimal scheduling of electric vehicles under grid capacity constraints and compares the trade-off between the convergence speed and the amount of communication required. However, this study only considers different combinations of two algorithms as well as considers linear capacity constraints and not the nonlinear transformer dynamics.

While many papers are devoted to coordinated charging of individual, residential EVs, fewer papers consider hubs of commercial EVs, such as school buses or delivery trucks. One such paper [32], aggregates PEVs and optimizes the lowest electricity charging cost solution under some linearized power flow constraints. Another [33], studies time of use pricing for a parking garage of electric vehicles. Others coordinate aggregate EVs for use as a virtual battery [34,35] or for frequency control [36]. This work will look specifically at how the electric vehicle hubs can meet their needs while respecting a transformer's temperature limit.

1.3 Research Objectives and Contributions

With this work, we build on the work from [37] but start with a nonlinear model for the transformer dynamics. While most previous works on electric vehicle charging (EVC) control selects one method that fits a specific needs, this work aims to compare multiple distributed methods and study the trade-offs between information sharing, performance, and computational processing. Including a novel distributed optimization method [38] and an iterative-free distributed method [39] adds control schemes which have not been analyzed for the EVC under dynamic multi-period coupling constraints. In addition, we add the second case study of the hub charging problem to give an example of a different application of the EVC problem. By introducing the hub charging problem, we are able to compare the algorithms across multiple case studies and contrast an application where privacy is the main priority to a commercial setting.

1.4 Thesis Outline

First, in Chapter 2 we review relevant information about transformers, electric vehicles and optimizing their charging. In Chapter 3, we formulate the neighborhood EV charging problem and compare four distributed algorithms. Chapter 4 follows this with the second case study where we apply the same four distributed algorithms to the hub charging problem. The distributed algorithm's results from the two case

studies are compared in depth in Chapter 5. We then conclude the work and discuss recommendations for further research in Chapter 6.

1.5 NOTATION

Brackets are used for time steps (e.g. $x[k]$ is the x value at the kth time step). Bold variables are vectors over all K time steps (e.g. $\mathbf{x} := \mathrm{col}\{x[0], x[1], \ldots, x[K]\}$) and non-bold variables are scalars. Superscript in parenthesis is used for iteration count (e.g. $\lambda^{(p)}$ is the λ value at the pth iteration).

Variable	Description	Domain	Units
\multicolumn EVC System Knowns			
N	Number of EVs	$\mathbb{Z}_+$	
$T_a[k]$	Ambient temperature at time k	$\mathbb{R}_+$	°C
$i_d[k]$	Background demand at time k	$\mathbb{R}_+$	kA
$T^{\max}$	Transformer temperature limit	$\mathbb{R}_+$	°C
γ	Ohmic losses-to-temp	$\mathbb{R}_+$	$^{°C\Omega}/_{kW}$
τ	Temp time constant	$\mathbb{R}_+$	
ρ	Ambient-to-temp losses	$\mathbb{R}_+$	
K	Optimization horizon length	$\mathbb{Z}_{++}$	# of time steps
Δt	Time step length	$\mathbb{R}_{++}$	Seconds
EV Specific Parameters			
$i_n^{\max}$	n^{th} EV current limit	$\mathbb{R}_+$	kA
α_n	n^{th} EV charging efficiency	[0,1]	
β_n	n^{th} EV battery size	$\mathbb{R}_+$	J
η_n	n^{th} EV normalized battery size	$\mathbb{R}_+$	$^1/_{kA}$
$\bar{s}_n$	Minimum SoC for n^{th} EV	[0,1]	
$\bar{k}_n$	Time step to reach minimum SoC	[0,K]	
Q_n	Penalty on partial SoC for n^{th} EV	$\mathbb{R}_+$	
R_n	Penalty on local power flow n^{th} EV	$\mathbb{R}_+$	

Table 1.1: Notation Used

CHAPTER 2

REVIEW OF PRELIMINARIES

In this chapter we will review theory behind transformer's and their temperature dynamics. Then, we will explain the dynamics of electric vehicle charging and how to optimally schedule them. Finally, we will review how this optimization problem can be decoupled into small problems.

2.1   TRANSFORMERS AND THEIR LIMITS

Power transformers are an important piece of the electric grid and allow efficient and low-loss transmission of power. At high voltages, low current levels can be maintained which results in low power losses (represented by I^2R). Transformers enable the conversion of electricity to high voltage before transmission and the conversion to lower voltage closer to where the power is being consumed. While the grid is adding distributed generation that allows for power to be generated closer to where it is consumed, transformers will still play a large role in the future electric grid. One scenario will be transporting energy from pockets of large utility-scale renewable

installations to pockets of large load.

Transformers are given a power rating, usually in kVA, which determines the maximum current at a given voltage. In addition, practical transformers have nonzero resistance and will tend to heat up as more current passes through. The limit to the transformer's temperature is often referenced in terms of a maximum hot spot temperature. When a transformer's temperature limit is exceeded, there is an increase in the degradation of the transformer and the lifespan decreases. The increase in temperature is a function of the thermal resistance of the transformer and the power loss. The thermal resistance, which is the resistance from the external ambient to the central hot spot, unfortunately, is difficult to measure with high accuracy.

The standard for transformer thermal modeling given a load history is in IEEE Guide to Loading Mineral-Oil Immersed Transformers Annex G [40] which is a complex, high-order, nonlinear model. However, simpler models do exist for approximating these dynamics. For this work, we use a first order quadratic model and further approximate with a piece-wise linear formulation.

2.2 Electric Vehicle Charging

As electric vehicle adoption has increased and automotive manufacturers have committed more and more to an electric future, the availability and options for how to charge electric vehicles have grown. Owners of electric vehicles can choose to charge at their home, at a public charging station, or at their work if charging stations are available. There are three main types of charging connections which results in three levels of charging. Level 1 charging is connecting the electric vehicle to a standard

8

120V outlet. With a charging power around 1kW this is the slowest charging mode and can take more than 12 hours to fully charge depending on the battery size. Level 2 charging supplies 240V and requires additional hardware but can charge at higher power (3-20kW but typically closer to 7kW). Level 2 charging is most often used in homes of private electric vehicle owners as well as at work and public charging stations. Finally, Level 3 charging, also known as fast charging or DC fast charging, offers the fastest method to charge. These use DC power and can charge at 50-120 kW with currently available technology. DC fast chargers are becoming more available at public stations as part of charging networks but require too high voltage to be installed at the average home.

While electric vehicles allow consumers to break off from their consumption and purchase of gasoline, they still have to consider the purchase of electricity for their vehicle. For private owners, charging at home will usually just add on to their electricity bill, however, some utilities are beginning to allow for a separate rate for EV charging. Some companies are now offering free electric vehicle charging as an employee benefit which is the ideal option financial if available. Those who want to make use of charging stations will have to decide between networked stations and non-networked stations. Charging networks are managed by charging network operators that usually require users to have a membership before using their stations. There are three main fast charging standards that are used in charging networks and electric vehicles are only compatible with one of them, adding even more complexity for users.
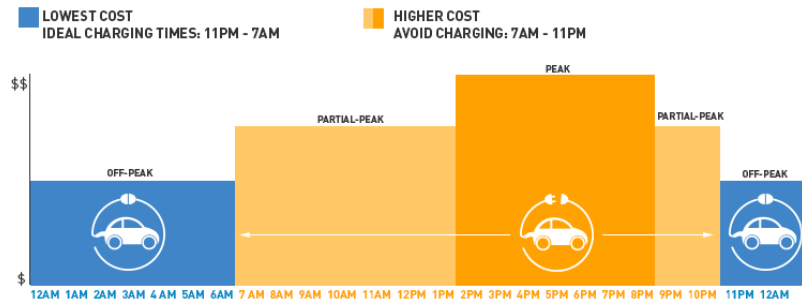
Figure 2.1: PG&E Time of Use Rate[1]

2.3 Optimal Scheduling of Electric Vehicles

With the introduction of a large population of electric vehicles charging in the same general area, we can start to consider coordinating the charging of electric vehicles. This becomes a resource allocation problem and involves finding the optimal schedule for charging. There are many different goals of such a problem depending on the real world application and from whose perspective you view the problem from. For instance, an electric vehicle owner might want to schedule their charging when electric prices are lowest if they are on a time of use rate tariff (see Fig. 2.1) or exposed to real-time prices. The grid operator might want to maximize the distance from any grid or device limits in order to maintain the reliability of the grid. A company that owns an electric fleet might care most about the quality of service to make sure that all vehicles have the minimum charge to complete their routes.

One method for solving the electric vehicle charging problem described above is to do the coordinating step in the cloud. This would involve having all relevant entities

---

[1]Image from: PG&E Website
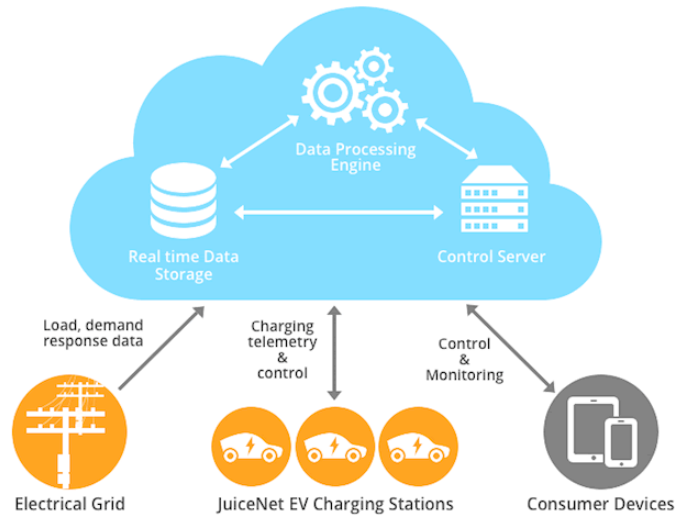
Figure 2.2: Cloud-based EV Charging System[2]

transmit their real-time data to the cloud, have a coordinator solve a problem, and then send the optimal solution back to the devices. A graphical representation of this can be seen in Fig. 2.2. There are a few downsides to this approach such as it has a very large communication overhead and has no protection of information. An alternative approach to solve the electric vehicle scheduling problem is through decomposition.

Decomposition is the general process of taking a problem, breaking it up into small problems, and then solving the small problems in order to get the solution for the original problem. One motivation for this approach is that the local problems can be solved in parallel which can result in faster solve times when compared to the original problem. Another reason to use decomposition is that the resulting algorithms can be implemented in a decentralized way which can be beneficial for various reasons including reduced communication and privacy concerns. We will utilize decomposition to solve the EV charging problem using different algorithms.

---

[2]Image from: JuiceNet Website

11

Chapter 3

Electric Vehicle Charging

Problem

This chapter contains the main electric vehicle charging problem we are trying to solve. We will introduce the models and formulate the nonlinear centralized problem. Then, we will perform a relaxation and a decomposition and run simulations comparing four different distributed algorithms. After a discussion of the results, we provide supplementary analysis on some important aspects of the problem.

3.1 System Models & Optimization

Consider a finite collection of N EVs charging at Level 2 charging stations that are served by the the same distribution-level substation transformer. Between any charger and the substation transformer is a pole-top transformer, as shown in Fig. 3.1. A current-based, transformer temperature model is used in the primal EVC formulation to keep the transformer hot-spot temperature below limits while satisfying the local
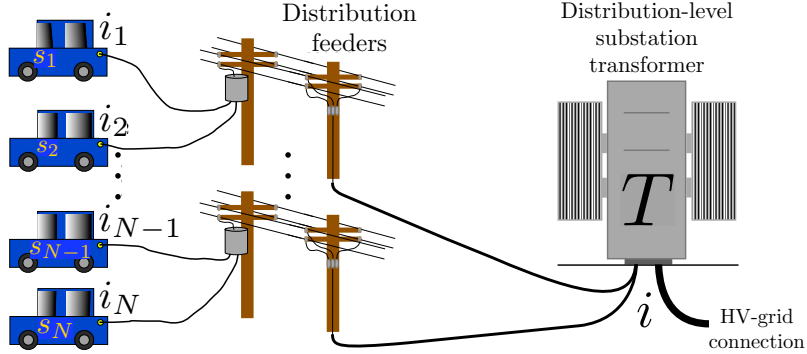
Figure 3.1: System Model

EV user constraints. The goal is to dynamically control the charging of all EVs under the transformer temperature limit. The many constraints and multi-period objectives give rise to a receding-horizon, model-predictive control (MPC) problem that is described at each time instance by an optimization problem of the following general form:

$$
\begin{aligned}
\min_{u} \quad & f_0(\mathbf{x}, \mathbf{u}) \\
s.t. \quad & f_i(\mathbf{x}, \mathbf{u}) \leq 0 \\
& h_i(\mathbf{x}, \mathbf{u}) = 0 \\
& \mathbf{x} \in [\mathbf{x}^{\min}, \mathbf{x}^{\max}]; \ \mathbf{u} \in [\mathbf{u}^{\min}, \mathbf{u}^{\max}],
\end{aligned}
\tag{3.1}
$$

where dynamic state $\mathbf{x} \in \mathbb{R}^{(N+1)K}$ represents the states of charge (SoCs) for all N EVs and the transformer temperature over the K timesteps in the prediction horizon[1]. The control input $\mathbf{u} \in \mathbb{R}^{NK}$ includes the EV charging rates. Constraints f_i and h account for inequality and equality constraints, respectively, while the box constraints capture state and control input limitations. The next sections make f_0, f_i, h_i explicit and

---

[1]In this work, the control and prediction horizons are assumed identical as the focus herein is on comparison privacy, performance, and processing across different algorithms.

couple charging rates, SoC, and transformer temperatures, as well as, the objective function that translates EV owner preferences into control objectives.

3.1.1 TRANSFORMER TEMPERATURE DYNAMICS

We will start with the simplified first order, quadratic model that was developed in [41] which can be seen in equation (3.2).

$$\dot{T}(t) = aL(t)^2 - b[T(t) - \tilde{T}_a(t)] + \tilde{c} \tag{3.2}$$

where $T(t)$ is the hot spot temperature, $L(t)$ is the power load, and $\tilde{T}_a(t)$ is the ambient temperature at time t. The constant coefficients a, b, and $\tilde{c}$ represent the effects of conduction, convection, and radiation, respectively. These parameters may be estimated from experimental data (as done in [41] with genetic programming) or from manufacturer spec sheets. In this manuscripts, the parameters are scaled versions of those in [41] with the additional qualification that the resulting model has a step-response that matches the timescale of the temperature responses given in spec sheets for similar MVA-scale transformers.

The differential equation in (3.2) has the solution

$$T(t) = e^{-b(t-t_0)}T(t_0) + \int_{t_0}^{t} e^{-b(t-\phi)}v(\phi)d\phi \tag{3.3}$$

where $v(\phi) = aL(\phi)^2 + b\tilde{T}_a(\phi) + \tilde{c}$. We would like to discretize this equation to be used in our simulations by plugging in $t = (k+1)\Delta t$ and $t_0 = k\Delta t$ where $k \in \{0, K\}$ are discrete time steps and Δt is the length of the time step.

$$T[(k+1)\Delta t] = e^{-b((k+1)\Delta t - k\Delta t)}T[k\Delta t] + \int_{k\Delta t}^{(k+1)\Delta t} e^{-b((k+1)\Delta t - \phi)}v(\phi)d\phi \qquad (3.4)$$

$$T[k+1] = e^{-b\Delta t}T[k] + e^{-b(k+1)\Delta t} \int_{k\Delta t}^{(k+1)\Delta t} e^{b\phi}v(\phi)d\phi \qquad (3.5)$$

We need to discretize $v(\phi)$, which we will do with a zero order hold by setting $v(\phi)$ to $v[k]$.

$$T[k+1] = e^{-b\Delta t}T[k] + e^{-b(k+1)\Delta t} \int_{k\Delta t}^{(k+1)\Delta t} e^{b\phi}v[k]d\phi$$

$$T[k+1] = e^{-b\Delta t}T[k] + e^{-b(k+1)\Delta t} \left[\frac{e^{b\phi}}{b}\right]_{k\Delta t}^{(k+1)\Delta t} v[k]$$

$$T[k+1] = e^{-b\Delta t}T[k] + \frac{1}{b}e^{-b(k+1)\Delta t}[e^{b(k+1)\Delta t} - e^{bk\Delta t}]v[k]$$

$$T[k+1] = e^{-b\Delta t}T[k] + \frac{1}{b}[1 - e^{-b\Delta t}]v[k]$$

Proof that this is an accurate discretization can be seen in 3.2. Adding back in $v[k]$ and simplifying constants gives us

$$T[k+1] = \tau T[k] + \tilde{\gamma}(L[k])^2 + \rho(\tilde{T}_a[k] + c) \qquad (3.6)$$

for $k = 0, \ldots, K-1$ and initial measure temperature at $T[0] = T_{\text{meas}}$ where $\tau = e^{-b\Delta t}$, $\rho = 1 - \tau$, $c = \frac{\tilde{c}}{b}$ and $\tilde{\gamma} = \frac{\rho}{b}$.

We would like to use a current based model instead of a power based model. We assume a constant voltage, V_{AC}, and rewrite in terms of total current

$$T[k+1] = \tau T[k] + \gamma(i_{\text{total}}[k])^2 + \rho(T_a[k]) \quad \forall k = 0, \ldots, K-1 \qquad (3.7)$$
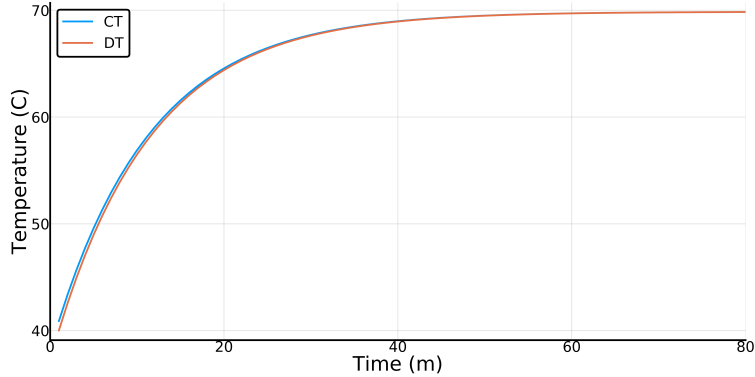
Figure 3.2: Comparison between Continuous and Discrete Transformer Hot Spot Temperature Dynamics

where $\gamma = \tilde{\gamma} V_{\mathrm{AC}}^2$ and $T_a[k] = \tilde{T}_a[k] + c$.

In addition, we are assuming that there are some limits to the hot spot temperature, $T^{\max}$, which would would like to operate below. Note that due to the $(i_{\mathrm{total}}[k])^2$ term this is a nonlinear equality constraint and is nonconvex.

3.1.2 EV DYNAMICS AND CONSTRAINTS

Using a similar approach we can discretize the continuous-time charging dynamics of the nth vehicle with current $i_n(t)$ at time t represented by

$$\dot{s}_n(t) = \tilde{\eta}_n V_{\mathrm{AC}} i_n(t) \tag{3.8}$$

where $\tilde{\eta}_n$ is the ratio of the vehicle's charging efficiency (α_n) to battery size (β_n) and V_{AC} is the constant RMS voltage at the EV. The discrete time equation is

$$s_n[k+1] = s_n[k] + \eta_n i_n[k] \tag{3.9}$$

16

for $k = 0, \ldots, K - 1$ and measured state of charge $s_n[0] = s_{\text{meas},n}$ where the domain of s_n is $[0, 1]$ and $\eta_n := \Delta t V_{\text{AC}}{}^{\alpha_n}/\beta_n$. Each vehicle has a maximum charging power $i_n^{\max}$.

3.1.3 EV OWNER PREFERENCES

The owners of the device determine a minimum state of charge $(\bar{s}_n)$ that must be met by a specific time step $(\bar{k}_n)$. The associated constraint for the nth vehicle is

$$s_n[k + 1] \geq s_n^*[k + 1] := \begin{cases} \bar{s}_n & k + 1 \geq \bar{k}_n \\ 0 & else \end{cases} \tag{3.10}$$

In addition, the user can set their preference for the trade-off between charging their device quickly and minimizing local battery wear and control effort. The user of the nth vehicle sets the ratio $\frac{Q_n}{R_n}$ to be large if they want to prioritize reaching full charge quickly (i.e., state penalty) or to be small if they prefer minimizing a proxy for battery wear and tear (i.e., control effort).

This ratio is used in the expression (J_n) which quantifies the value to the owner of the charging and state of charge schedule for the nth vehicle.

$$J_n(\mathbf{i}_n, \mathbf{s}_n) = \sum_{k=1}^{K}(s_n[k] - 1)^2 Q_n + \sum_{k=0}^{K-1}(i_n[k])^2 R_n \tag{3.11}$$

Summing over all N vehicles gives us a total performance metric which we will minimize in the optimization problem.

$$\min \sum_{n=1}^{N} J_n(\mathbf{i}_n, \mathbf{s}_n) \qquad (3.12)$$

This objective function is similar to a conventional linear quadratic regulator (LQR) that penalizes deviations in SoC from full and balances this SoC satisfaction against charging rates.

3.2 Nonlinear Central Problem Formulation

We now would like to formulate an optimization problem using the performance metric as the objective function. The open-loop optimal central problem is simply the combination of the above constraints and objective function for all devices and

time steps. This is a nonconvex problem due to the nonlinearity in (3.13d).

$$\min \ \sum_{n=1}^{N} J_n(\mathbf{i}_n, \mathbf{s}_n) \tag{3.13a}$$

$$\text{s.t.} \tag{3.13b}$$

$$i_d[k] + \sum_{n=1}^{N} i_n[k] = i_{\text{total}}[k] \tag{3.13c}$$

$$T[k+1] = \tau T[k] + \gamma(i_{\text{total}}[k])^2 + \rho T_a[k] \tag{3.13d}$$

$$T[k+1] \leq T^{\max} \tag{3.13e}$$

$$s_n[k+1] = s_n[k] + \eta_n i_n[k] \tag{3.13f}$$

$$s_n[k+1] \in [s_n^*[k+1], 1] \tag{3.13g}$$

$$i_n[k] \in [0, i_n^{\max}] \qquad\qquad T[0] = T_{\text{meas}} \tag{3.13h}$$

$$s_n[0] = s_{\text{meas},n} \tag{3.13i}$$

for all $k = 0, \ldots, K - 1$ and $n = 1, \ldots, N$.

Note that the only coupling between the transformer and EV dynamics is the equality constraint in (3.13c). Previous work in [37] had a temperature coupling constraint whereas this is a current or power coupling.

3.3   Convexification of NL Problem

The only non-linearity in the problem is the current squared in the transformer temperature dynamics (3.13d). We considered two different relaxations: a convex relaxation and a piecewise linear formulation.
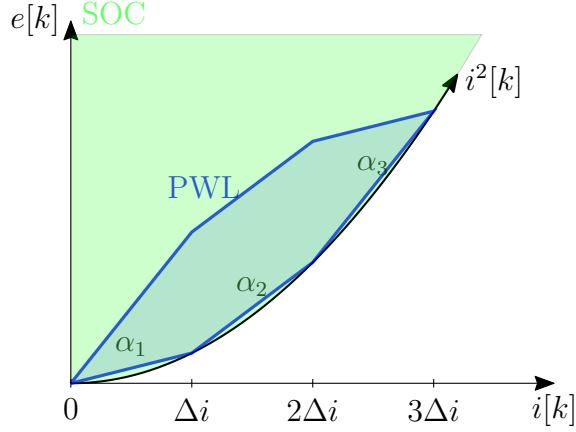
Figure 3.3: PWL Approximation (blue) and Convex Relaxation (green) of i^2

One approach is relaxing the quadratic equality (3.13d) to an inequality as seen in green in Fig. 3.3

$$T[k+1] = \tau T[k] + \gamma e[k] + \rho T_a[k] \tag{3.14}$$

$$e[k] \geq i_{\text{total}}^2[k] \tag{3.15}$$

The primal problem can now be cast as a second order cone program (SOCP).

Theorem 3.3.1. *At optimality, if $k > 0$ is the largest $k < K$ for which $T^*[k+1] = T^{max}$, then $e^*[l] = i_{total}^*[l]^2 \ \forall l \leq k$ and the convex relaxation is tight for all prior time-steps $l \leq k + 1$.*

Proof. The proof is based on KKT conditions, which are necessary and sufficient conditions for optimality since the primal problem satisfies Slater's constraint quali-fication and is convex. See Appendix A for detailed proof. □

Remark. *Note that for all remaining time-steps, $l > k$, the relaxation need not be tight as the coupling constraint is not binding (i.e., $T[l] < T^{max}, \forall l > k$). However,*

the effects of these "fictitious" losses, i.e., $\gamma(e[k] - i_{total}^2[k]) > 0$, are of no consequence to the charging control as they do not constrain the transformer.

The benefit of the convex relaxation approach is that this relaxation is exact to the nonlinear model. However, quadratic or conic constraints increases the complexity of complementary conditions and can lead to numerical difficulties. A different approach is the piece-wise linear (PWL) method as seen in blue in Fig. 3.3 which creates an quadratic problem and improves numerics of the problem. The quadratic problem is a subset of second-order cone problems meaning it is inherently less complex. As we develop a convex solver to handle the more generic problems, numerics become a challenge at scale. Another benefit of using the PWL approximation is that it will overestimate the transformer current, as a function of the number of segments, which beget an accurate, but conservative prediction of the transformer temperature. Therefore, for the remainder of this work, we will focus on the PWL implementation.

3.3.1 PIECEWISE LINEAR APPROXIMATION

Define $e[k]$ a piece-wise linear (PWL) approximation of $i_{\text{total}}[k]^2$ with M segment of equal width $\Delta i := \frac{I^{\max}}{M}$ where $I^{\max}$ is a realistic maximum transformer current

$$i_{\text{total}}[k]^2 \approx e[k] := \text{PWL}\{i_{\text{total}}[k]^2\} = \sum_{m=1}^{M} \alpha_m i_m^{PW}[k] \tag{3.16}$$

where the slope of segment m is defined by

$$\alpha_m = \frac{(m\Delta i)^2 - ((m-1)\Delta i)^2}{(m\Delta i) - ((m-1)\Delta i)} = (2m-1)\Delta i \tag{3.17}$$

Which gives us

$$e[k] = \Delta i \sum_{m=1}^{M} (2m-1)i_m^{PW}[k] \tag{3.18}$$

Using this in the transformer constraint,

$$T[k+1] = \tau T[k] + \gamma \left(\Delta i \sum_{m=1}^{M} (2m-1)i_m^{PW}[k] \right) + \rho T_a[k] \quad \forall k = 0, \dots, K-1 \tag{3.19}$$

The SOCP based proof in Theorem 3.3.1 is analogous to the proof of adjacency of the segments for PWL, therefore these constraints are not included in the PWL optimization.

Remark. *Upper bound on PWL error: since we are using equal width segments, the maximum error between the PWL approximation and the actual i^2 is just the maximum distance between the linear segment ($PWL(i)$) and the quadratic curve ($q(i)$) at the midpoint (i.e. $\frac{\Delta i}{2} := \frac{I^{max}}{2M}$).*

$$\epsilon_i^{max} = PWL\left(\frac{\Delta i}{2}\right) - q\left(\frac{\Delta i}{2}\right) = \frac{(I^{max})^2}{2M^2} - \left(\frac{I^{max}}{2M}\right)^2 \tag{3.20}$$

$$\Rightarrow \epsilon_i^{max} = \frac{(I^{max})^2}{4M^2}. \tag{3.21}$$

Multiplying by γ provides the upper bound on the corresponding temperature error:

$$\epsilon_T^{max} = \frac{\gamma(I^{max})^2}{4M^2}. \tag{3.22}$$

Even for a large $I^{max} = 0.72kA$ current with $\gamma = 15.74 {^\circ C - \Omega}/_{MW}$, and $M = 6$ segments, the maximum error between a PWL's linear prediction of the transformer temperature (T_{PWL}) and the quadratic temperature (T_q) for a single time step is

$\epsilon_T^{max} := T_{PWL}[k+1] - T_q[k+1] = 0.057°C$ *when the convex relaxation is tight. While this temperature error accumulates over time steps in the open loop problem, it also dissipates over time due to the $\tau < 1$ term. Therefore, the piece-wise linear approximation provides a feasible, robust estimate of the nonlinear temperature dynamics.*

3.3.2 PRIMAL CENTRALIZED PWL PROBLEM

Using the PWL relaxation gives a new central problem with a new transformer dynamic (3.19) which replaces (3.13d). In addition, we will need to rewrite the current coupling constraint between the PWL current segments and the EV currents

$$i_d[k] + \sum_{n=1}^{N} i_n[k] = \sum_{m=1}^{M} i_m^{PW}[k] \quad \forall k = 0, \dots, K-1 \tag{3.23}$$

Also, there are the limits on the piecewise segments

$$i_m^{PW}[k] \in [0, \Delta i] \quad \forall k = 0, \dots, K-1 \tag{3.24}$$

3.4 PROBLEM DECOUPLING

The centralized problem can be decomposed with the exception of the coupling constraint (3.23). We will use the dual decomposition method to create a distributed implementation. First, we consider the partial Lagrangian with respect to (3.23)

$$\mathcal{L}(\mathbf{i}_n, \mathbf{s}_n, \mathbf{i}_m^{PW}, \lambda) = \sum_{n=1}^{N} J_n(\mathbf{i}_n, \mathbf{s}_n) + \lambda^T \left(\mathbf{i}_d + \sum_{n=1}^{N} \mathbf{i}_n - \sum_{m=1}^{M} \mathbf{i}_m^{PW} \right) \quad (3.25)$$

$$= \sum_{n=1}^{N} \left(J_n(\mathbf{i}_n, \mathbf{s}_n) + \lambda^T \mathbf{i}_n \right) + \lambda^T (\mathbf{i}_d - \sum_{m=1}^{M} \mathbf{i}_m^{PW})) \quad (3.26)$$

where $\lambda \in \mathbb{R}^K$ is the Langrangian multipliers associated with (3.23). As seen in (3.26), the Lagrangian can be separated into local EV variables $\{\mathbf{i}_n, \mathbf{s}_n\} \in \mathbb{R}^{2NK}$ and transformer variables $\{\mathbf{i}^{PW}\} \in \mathbb{R}^{MK}$. If we now minimize (3.26) for a fixed λ then we minimize a separable objective subject to separable constraints. This means that the optimization problem decouples and can be done in parallel. Thus, the focus is now on how to update λ to which we develop and present three optimization-based, iterative methods and one iterate-free method.

3.5   Distributed Algorithms
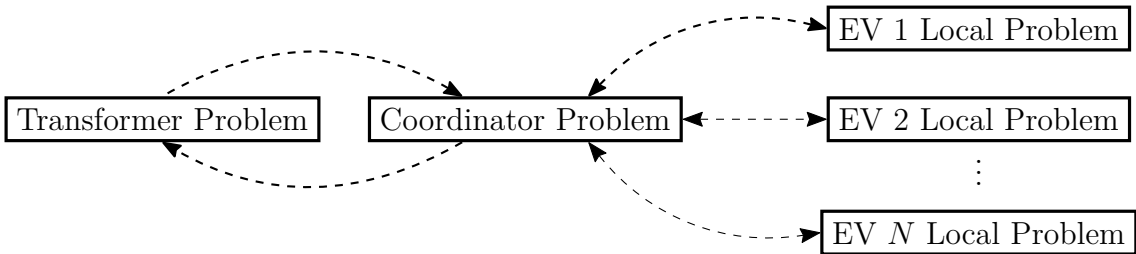
Figure 3.4: Graphic of Distributed Schemes. At its simplest (dual decomposition), there is only one piece of information being exchanged between problems and the coordinated problem is a projected gradient approach. ADMM slightly increases the information transferred, while ALADIN greatly increases the information transfers and the complexity of the coordinator problem by solving a QP.

Four different distributed schemes will be tested each with different requirements

on communication. Dual decomposition, ADMM, and ALADIN are all distributed optimization algorithms while PEM is an iterative-free control scheme and each has different requirements for the transformer, EV and coordinator problems seen in Fig. 3.4. Note that these distributed schemes are synchronous in that they require the communications from all local problems before continuing with the coordinator step. Literature exists that covers asynchronous distributed methods and gives guarantees under certain delays such as this article for asynchronous ADMM [42].

3.5.1 DUAL DECOMPOSITION

Algorithm 1 Dual Decomposition

Initialization: Initial guess of dual multiplier $\lambda^{(1)}$
Repeat: for $p <$ Max Iterations:

1. *Local EV Problem:* Solve for each $n \in N$

$$\mathbf{i}_n^{(p)} = \arg\min_{\mathbf{i}_n} \quad J_n(\mathbf{i}_n, \mathbf{s}_n) + (\lambda^{(p)})^T \mathbf{i}_n \tag{3.27}$$

$$\text{s.t.} \quad (3.13\text{f}), (3.13\text{g}), (3.13\text{h})$$

2. *Transformer Problem:*

$$(\mathbf{i}_m^{PW})^{(p)} = \arg\min_{\mathbf{i}_m^{PW}} \quad -(\lambda^{(p)})^T \sum_{m=1}^{M} \mathbf{i}_m^{PW} \tag{3.28}$$

$$\text{s.t.} \quad (3.19), (3.24), (3.13\text{e})$$

3. *Coordinator Problem:* Update dual variable

$$\nabla_\lambda \mathcal{L} = \sum_{n=1}^{N} \mathbf{i}_n^{(p)} + \mathbf{i}_d - \sum_{m=1}^{M} (\mathbf{i}_m^{PW})^{(p)} \tag{3.29}$$

$$\lambda^{(p+1)} = \lambda^{(p)} + \alpha^{(p)} \nabla_\lambda \mathcal{L} \tag{3.30}$$

Dual decomposition separates eq (3.26) and creates local linear problems and updates λ by dual ascent. Standard dual decomposition with dual ascent update

for separable problems is used as seen in [43] and applied in a similar problem in [37]. The iterative algorithm is described in Algorithm 1 with $\alpha^{(p)} = \frac{\alpha^0}{\text{ceil}(\frac{p}{\alpha_{rate}})}$ where $\alpha^0 = 10^4$ and $\alpha_{rate} = 2$.

3.5.2 Alternating Direction Method of Multipliers

Algorithm 2 ADMM

Initialization: Initial guess of dual multiplier $\lambda^{(1)}$ and auxiliary variables $\{\mathbf{v}_{i,n}^{(1)}, \mathbf{v}_{m,PW}^{(1)}\}$
Repeat: for $p <$ Max Iterations:

1. *Local EV Problem:* Solve for each $n \in N$

$$\mathbf{i}_n^{(p)} = \arg\min_{\mathbf{i}_n} \ J_n(\mathbf{i}_n, \mathbf{s}_n) + (\lambda^{(p)})^T(\mathbf{i}_n - \mathbf{v}_{i,n}^{(p)}) + \frac{\rho^{(p)}}{2}(\mathbf{i}_n - \mathbf{v}_{i,n}^{(p)})^2 \tag{3.31}$$

$$\text{s.t.} \quad (3.13\text{f}), (3.13\text{g}), (3.13\text{h})$$

2. *Transformer Problem:*

$$(\mathbf{i}_m^{PW})^{(p)} = \arg\min_{\mathbf{i}_m^{PW}} \ -(\lambda^{(p)})^T \sum_{m=1}^{M}(-\mathbf{i}_m^{PW} - (\mathbf{v}_m^{PW})^{(p)}) + \frac{\rho^{(p)}}{2}\sum_{m=1}^{M}(-\mathbf{i}_m^{PW} - (\mathbf{v}_m^{PW})^{(p)})^2$$

$$\tag{3.32}$$

$$\text{s.t.} \quad (3.19), (3.24), (3.13\text{e})$$

3. *Coordinator Problem:* Update primal and dual variables

$$\nabla_\lambda \mathcal{L} = \sum_{n=1}^{N} \mathbf{i}_n^{(p)} + \mathbf{i}_d - \sum_{m=1}^{M} (\mathbf{i}_m^{PW})^{(p)} \tag{3.33}$$

$$\lambda^{(p+1)} = \lambda^{(p)} + \frac{\rho^{(p)}}{K}\nabla_\lambda \mathcal{L} \tag{3.34}$$

ADMM builds on top of dual decomposition by augmenting the local objective functions using auxiliary variables. A separable ADMM approach is introduced in [44] and can be seen in Algorithm 2. $\rho^{(p)}$ starts at $\rho^{(1)} = 2 * 10^5$ and increments by

$\rho_{rate} = 1.02$ each iteration.

Note: Due to the sign of the objective function in the transformer problem, at the optimal solution $(\mathbf{i}_m^{PW}) = -(\mathbf{v}_m^{PW})$

3.5.3 Augmented Lagrangian based Alternating Direction Inexact Newton

Augmented Lagrangian based Alternating Direction Inexact Newton method (ALADIN) is a relatively new distributed optimization algorithm [38]. The method decomposes the central optimization problem by having each agent solve its own local quadratic program (QP) based on an initial guess of auxiliary variables and the Lagrange multiplier of the coupling constraint. A slight abuse of notation will be used in the algorithm explanation. Consider general optimization variable x. Then, H_x represents the Hessian of the original objective function with respect to optimization variable x where

$$x \in \mathcal{X} := \left\{ \{\mathbf{i}_n\}_{n=1}^N, \{\mathbf{s}_n\}_{n=1}^N, \{\mathbf{i}_m^{PW}\}_{m=1}^M, \mathbf{T} \right\} \subset \mathbb{R}^K$$

with $|\mathcal{X}| = 2N + M + 1$. The primal solution from each local EV and transformer problem is shared with the coordinator. In addition, the gradient of the objective function $(g_x = \frac{dJ_n}{dx})$ and the Jacobian of the box constraints, $x \in [x^{\min}, x^{\max}]$ is given by $C_x = [-1, 1]^\top$ for each local variable $\{\mathbf{i}_n, \mathbf{s}_n\}$ and $\{\mathbf{i}_m^{PW}, \mathbf{T}\}$. The coordinator then combines the local information into a large QP to updates the auxiliary variables and dual multiplier. The ALADIN algorithm used for the EV charging problem for a single MPC time step t is seen in 3.

Algorithm 3 ALADIN (for time instance t)

Initialization: Initial ($p \equiv 0$) guess of dual multiplier $\lambda^{(0)}$ and all four auxiliary variables $\{\mathbf{v}_{i,n}^{(0)}, \mathbf{v}_{s,n}^{(0)}, \mathbf{v}_{i,PW}^{(0)}, \mathbf{v}_T^{(0)}\}$

Repeat for p:

1. *Solve local EV problems:* for each $n \in N$

$$\mathbf{i}_n^{(p)} = \arg\min_{\mathbf{i}_n} \ J_n(\mathbf{i}_n, \mathbf{s}_n) + (\lambda^{(p)})^T \mathbf{i}_n + \frac{\rho_{\text{ALAD}}\sigma_{i,n}}{2}(\mathbf{i}_n - \mathbf{v}_{i,n}^{(p)})^2 + \frac{\rho_{\text{ALAD}}\sigma_{s,n}}{2}(\mathbf{s}_n - \mathbf{v}_{s,n}^{(p)})^2$$

    s.t. $(3.13\text{f}), (3.13\text{g}), (3.13\text{h})$

2. *Solve local transformer problem:*

$$(\mathbf{i}_m^{PW})^{(p)} = \arg\min_{\mathbf{i}_{pw}} \ -(\lambda^{(p)})^T \sum_{m=1}^{M} \mathbf{i}_m^{PW} + \frac{\rho_{\text{ALAD}}\sigma_Z}{2}(\mathbf{i}_m^{PW} - \mathbf{v}_{i,PW}^{(p)})^2 + \frac{\rho_{\text{ALAD}}\sigma_T}{2}(\mathbf{T} - \mathbf{v}_T^{(p)})^2$$

    s.t. $(3.19), (3.24), (3.13\text{e})$

3. *Solve coordinator problem:*

$$\min \sum_{i=1}^{|\mathcal{X}|} \sum_{n=1}^{N} \left(\frac{1}{2}\Delta\mathbf{x}_i H_{x_i}\Delta\mathbf{x}_i + g_{x_i}^{(p)}\Delta\mathbf{x_i} \right) \tag{3.35a}$$

$$\text{s.t. } i_d[k] + \sum_{n=1}^{N}(i_n^{(p)}[k] + \Delta i_n[k]) = \sum_{m=1}^{M} \left((i_m^{PW})^{(p)}[k] + \Delta i_m^{PW}[k] \right) \mid \lambda_{QP}[k] \tag{3.35b}$$

$$\Delta T[k+1] = \tau\Delta T[k] + \gamma \left(\Delta i \sum_{m=1}^{M}(2m-1)\Delta i_m^{PW}[k] \right) \tag{3.35c}$$

$$\Delta s_n[k+1] = \Delta s_n[k] + \eta_n\Delta i_n[k] \tag{3.35d}$$

$$C_{x_i}^{(p)}\Delta\mathbf{x}_i \leq 0 \quad \forall i = 1, \dots, |\mathcal{X}| \tag{3.35e}$$

    for all $k = 0, \dots, K-1$

4. **if**

$$\left\| i_d[k] + \sum_{n=1}^{N} i_n[k]^{(p)} - \sum_{m=1}^{M}(i_m^{PW})^{(p)}[k] \right\|_1 \leq \epsilon_1 \text{ and} \tag{3.36}$$

$$\left\| \lambda^{(p)} - \lambda^{(p-1)} \right\|_2 \leq \epsilon_2 \tag{3.37}$$

    then exit with $x^* = x^{(p)}$ and $i_n^*[0]$ is implemented in EVs.

5. *Update dual variable and auxiliary variables*

$$\lambda^{(p+1)} = \lambda_{QP} \tag{3.38}$$

$$\mathbf{v}_{x_i}^{(p+1)} = \mathbf{x_i}^{(p)} + \Delta\mathbf{x_i} \quad \forall i = 1, \dots, |\mathcal{X}| \tag{3.39}$$

$$p \to p + 1$$

A slight alteration to the ALADIN formulation was used which changes the Jacobian approximation constraints (3.35e) to be inequalities from their original equality constraints. This relaxation allows the local variables to move asymmetrically away from its bound instead of fixing all variables that are at their upper or lower limit.

ALADIN provides a systematic approach to decomposing our large central QP into many smaller local QPs and a coordinator QP. However, the information required from the sub-problems is significant and the coordinator problem is computationally intensive. To contrast the information and processing intense method that is ALADIN, we next present a novel, EV-speciifc, and predictive version of the recently developed packetized energy management (PEM).

3.5.4   PEM with Dynamic Constraints

PEM represents a computationally and informationally light demand-side coordinating scheme for scheduling (in real-time) many distributed resources, such as EV charging. The scheme uses a probabilistic, packetized approach similar to modern communication networks [39] to dynamically prioritize demand-side resources. The full PEM algorithm used for the EV charging problem for a single MPC time step t is seen in 4. Each local "packetized" device can infer or measure its *energy need*, which is mapped to a prescribed probability of requesting a fixed-duration (δ) packet of energy (e.g., a δ time step, constant-amperere charging epoch). The request is submitted to the coordinator, which takes into account real-time and/or predicted transformer conditions to either accept or reject the packet in order to maintain the transformer temperature within its limits. To ensure quality-of-service for the device owner, opt-out logic enables devices with extreme energy needs to temporarily exit

the scheme and recover SoC in a timely manner.

Local EV Problem

The PEM scheme does not require solving a local optimization problem. Instead, a "packetized" EV charger is assumed capable of accurately inferring the EV's state-of-charge (SoC) and time until departure. Based on these two updates, the EV (asynchronously, on its own clock) calculates its energy need with the ratio

$$\text{ratio}_n := \frac{\bar{s}_n - s_{\text{meas},n}}{\eta_n i_n (\bar{k}_n - k)} \in \mathbb{R}.$$

If the ratio > 1, then the time remaining is not sufficient to provide the desired energy, even if charging for the entire remaining duration. Thus, if ratio reaches or initially exceeds unity, then the device will automatically opt out ($\text{Req}_n < 0$) and continuously charge until the time of departure. Thus, opting out represents a background disturbance to the fleet of packetized EV chargers, which reduces the number of packets that can be accepted by the coordinator. When the ratio remains in $[0, 1]$, the ratio value is mapped to a probability of requesting a packet (($\text{Req}_n \in \{0, 1\}$), e..g, please see Algorithm 4. The probability of requesting a packet depends on the ratio and a pre-specified mean time-to-request (or mttr) for a specific ratio value set-point ($\hat{r}_{\text{set},n}$). As $\text{ratio}_n[k] \to 0/1$, the probability of requesting approaches $0/1$. Of course, while a device is "consuming" an energy packet, it is ineligible to request another packet, so $\text{Req}_n[k]$ is set to the negative of the remaining packet duration.

If the ratio is such that EV requests a packet ($\text{Req}_n \equiv 1$) and is notified that its packet is accepted, the EV charges at a pre-specified current for δ time steps.

If the ratio is negative ($\text{Req}_n \equiv 2$) then the EV's SoC exceeds its desired energy target, which means that the EV's "energy need" has been satisfied and any future requests from this EV automatically becomes a low-priority request. For the results shown in Case Study 1, $\delta = 2$, $mttr = \Delta t \delta = 2$ timesteps (i.e., $2 \times 180 = 360$s), and $\hat{r}_{\text{set},n} = 0.10$. The decision of these parameters is discussed in Section 3.7.5

Coordinator Problem

The coordinator logic is developed to keep the temperature within limits while accepting as many packet requests as possible. Since temperature is a dynamic state and prior work with PEM and EVs focused on static power or current limits, one major contribution of this paper is the extension of PEM for scheduling under dynamic state constraints. This section describes a novel, predictive, and synchronous coordinator formulation for PEM that utilizes a simple mixed-integer QP (MIQP) to determine which requests are accepted and denied.

To do so, first define the set of all devices that do not request a packet ($\text{Req}_n[t] \equiv 0$) at time t as $\mathcal{E}_0$. Define δ sets for $\mathcal{Y}_k$ for the devices that are "locked in" at times $t+1, \ldots, t+\delta$ either from still consuming an energy packet or from opting out. This set captures the predicted populations of devices that must charge over the next δ timesteps. The devices that request a packet at time t make up the set $\mathcal{E}_1$. Lastly, define $\mathcal{E}_2$ as the set of EVs that have already reached their SoC target, but are not at 100% SoC.

A mixed integer quadratically constrained problem is solved to determine which EVs have their packets accepted and rejected. Since the problem is small due to the short prediction horizon, the QCQP relaxation in (3.15) is used instead of a PWL

31

Algorithm 4 PEM algorithm (for time instance t)

Local EV Problem: solve for each $n \in N$
    if Consuming Packet **then**
        $\text{Req}_n[t] = -$ duration remaining for packet
    else if $s_{\text{meas},n}[t] = 1$ **then**   ▷ EV at 100%
        $\text{Req}_n[t] = 0$
    else if $s_{\text{meas},n}[t] \geq \bar{s}_n$ **then**   ▷ EV past desired SoC
        $\text{Req}_n[t] = 2$
    else
        $\text{ratio}_n[t] = \dfrac{\bar{s}_n - s_{\text{meas},n}[t]}{\eta_n * i_n^{\text{est}}(\bar{k}_n - t)}$
        if $\text{ratio}_n[t] \geq 1$ **then**
            $\text{Req}_n[t] = -\delta$ ▷ EV opts out
        else
            $\mu[t] = \frac{1}{mttr} \frac{\text{ratio}_n[t]}{1 - \text{ratio}_n[t]} \frac{1 - r_{\text{set},n}}{r_{\text{set},n}}$
            $P_n[t] = \min\{\max\{1 - e^{-\mu[t]\Delta t}, 0\}, 1\}$
            $\text{Req}_n[t] = \begin{cases} 1, & rand() < P_n[t] \\ 0, & else \end{cases}$

End
Transformer Problem:
    Send T_{meas} to Coordinator
End
Coordinator Problem:
Update sets $\mathcal{E}_0, \mathcal{E}_1, \mathcal{E}_2, \mathcal{Y}_k$
Solve MIQP:

$$\mathbf{u}_{\text{ch}}^* = \arg \max_{T_{est}, u_n} \sum_{k=0}^{\delta-1} \left(\sum_{n \in \mathcal{E}_1} u_n[k] + \omega_E \sum_{n \in \mathcal{E}_2} u_n[k] \right) - \omega_S T_{slack} \tag{3.40}$$

$s.t$

$$T_{est}[0] = T_{\text{meas}}[t] \tag{3.41}$$

$$T_{est}[k+1] \geq \tau T_{est}[k] + \rho T_a[t+k] + \gamma \left(\sum_{n=1}^{N} u_n[k] i_n^{\text{est}} + i_D[t+k] \right)^2 \quad \forall k = 0, \dots, \delta-1 \tag{3.42}$$

$$T_{est}[k] \leq T^{\max} + T_{\text{slack}} \quad \forall k = 1, \dots, \delta \tag{3.43}$$

$$u_n[k] = 1 \quad \forall n \in \mathcal{Y}_k \; \forall k = 0, \dots, \delta-1 \tag{3.44}$$

$$\sum_{k=0}^{\delta-1} \sum_{n \in \mathcal{E}_0} u_n[k] = 0 \tag{3.45}$$

$$u_n[k] \in \{0,1\} \quad \forall n = 1, \dots, N \; \forall k = 0, \dots, \delta-1 \tag{3.46}$$

Select EVs to receive charge:
    $\text{Rec}_n[t] = u_{\text{ch},n}^*[0]$ ▷ From optimal solution pool
End
---

formulation. No numerical issues were encountered. The requests from $\mathcal{E}_2$ are de-prioritized by use of a scaling factor ($\omega_E := \min\{1/(NK), 1/(4N)\} << 1$) in the objective function. To ensure a solution always exists, a slack variable is added to the temperature limit and penalized in the objective function ($\omega_S >> 1$).

Finally, in the MIQP, any devices that do not send a request or opt-out are assumed to stay in their previous logic state, which could be $\text{Req}_n[k] \in \{< 0, 0, 2\}$. This ensures an information-light implementation whereby only logic state changes are communicated. Furthermore, the MIQP depends on an estimate of the current demanded from device n. This estimate could be exact if the information is included in the request or may be approximated via machine learning on the population. In this work, we assumed the former. After solving the MIQP, the optimal solutions are pooled and a random solution is chosen as $\mathbf{u}_{\text{ch}}^*$, which represents the vector of the coordinator's recommendations for each device (Rec_n). To keep communication overhead low for this predictive implementation of PEM, only devices whose logic state undergoes a transition should be updated.

3.6 SIMULATIONS AND RESULTS

Now that we have defined the distributed methods to be used to coordinate the optimal EV charging schedule, the following section explains the scenario used, how the algorithms are implemented in an MPC controller, and the results of the simulations. The schematic of the system we are modeling and solving is shown in Fig. 3.1.

3.6.1   SCENARIO SETUP

This subsection will go over the assumptions used and why they create a realistic scenario to simulate. A summary of the parameters can be seen in Table 3.1, 3.2, and 3.3.

Simulation Time Horizon

As most residential EV owners will utilize home charging for the majority of their EV energy, we expect the peaks to occur in the evening [7–9]. Our simulation will run from when most vehicles arrive at home through when most will have left for work the next day, 8 PM to 10 AM. We want to use a time step that is much smaller than the time constants of the transformer. In general, the time constant of large transformers is on the scale of 30 minutes , so a time step of 180 seconds will be adequate. Using $Ts = 180s$ gives us a total number of time steps of $\frac{14hr}{180s} = 280$. We will use an 8-hour prediction window for each open loop optimization step in the model predictive controller so $K = \frac{8hr}{180s} = 160$

Transformer and Electrical Grid Setup

We would like to model a system with one medium to large distribution-level substation transformer and pole-top transformers as seen in Fig. 3.1. We chose to use a 10MVA three-phase transformer with low side voltage of 8.32 kV and pole-top transformers that reduce this voltage to 240 V for distribution to residential buildings. It is worth noting that we assume the pole top transformers will not overload although this is another potential issue that will be needed to address with the increased adoption

of electric vehicles (See [41]).

Transformer Limit and Initial Temperature

For short term overloading, we would like to keep the hot-spot temperature of the transformer under 120°C in order to reduce the aging affects [45,46]. We will initialize the simulation with the hot spot temperature 65°C below the maximum temperature.

Transformer Parameters

As mentioned in the Review of Preliminaries, Section 2.1, we would like to model and limit the hot-spot temperature in the distribution level substation transformer. The IEEE standard, Annex G, is complicated and will be difficult to simulate in a reasonable amount of time. Instead, we will use the first order, quadratic differential equation (3.2). We started with equations used in [41] scaled them to a 10MVA transformer and modified them until we saw a 65°C temperature rise above ambient at 1 p.u. loading as well as matching temperature responses to [47,48]. Our continuous parameters for the power dynamics in (3.2) are $a = 7.92 * 10^{-8}$, $b = 0.0298$, and $\tilde{c} = 0.89$. The equivalent discrete time current equation parameters are $\gamma = 0.131$, $\tau = 0.914$, and $\rho = 0.086$.

Ambient Temperature

The scenario we will use in the simulation is one for a hot summer night. The temperature starts at 30C (86F) and hits a low of 27C (81F) before rising again in the morning (see Fig. 3.5 (b)).

35
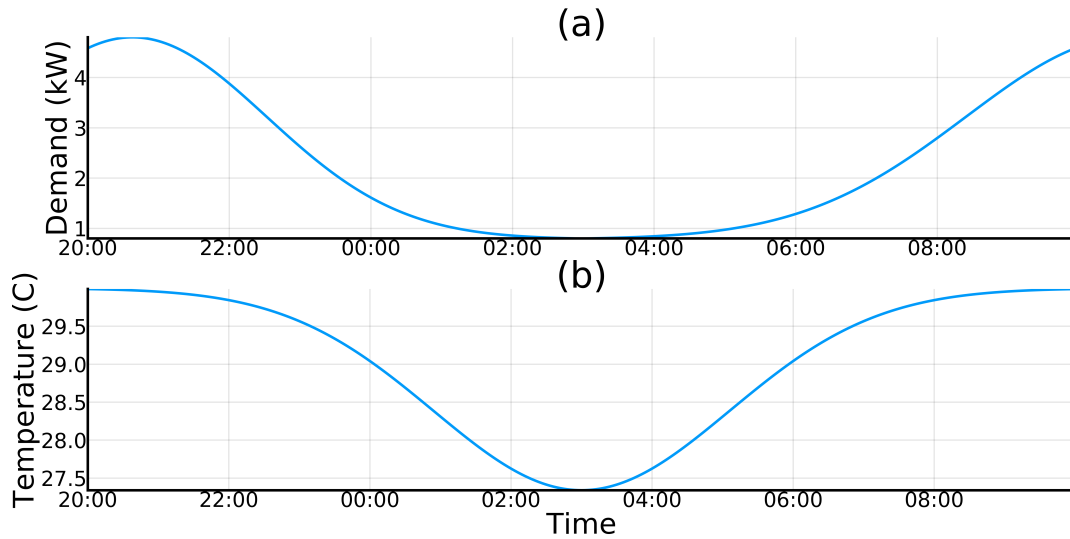
Figure 3.5: Background Demand for a Single House (a) and Ambient Temperature (b)

Background Demand

The three-phase transformer that was chosen gives us 3.33 MVA per phase of the total rated capacity. If we assume that each residential home peaks at 3.5 kVA [49, 50] this transformer would be rated for about 1,000 houses. For this simulation, we will assume that the houses are using more power than usual due to the excessive heat and they peak at 5kVA with an average around 2kVA. The inflexible background demand for a single residential building can be see in Fig. 3.5 (a).

Electric Vehicle Penetration

We have chosen to simulate a scenario with 10% EV penetration where penetration is defined as the percentage of electric meters (houses) servicing a single EV. A few other papers [49,51] have seen this is the threshold where transformer overloads might start occurring. For our 1,000 home scenario, we now have 100 EVs total in the simulation.

Electric Vehicle Efficiency

The charging efficiency is assumed to be constant for each vehicle and drawn from a uniform distribution between 80% and 90% [52]. While this does simplify nonlinearities when it comes to the impacts of temperature [52], current [52], and state of charge [53] on the charging efficiency, these affects are relatively small and for the purpose of the study will not change the analysis of the coordination methods.

Electric Vehicle Battery Size

The vast majority of plug-in electric vehicles on the road and sold today are a combination of the Nissan Leaf, Chevrolet Bolt, and the Tesla fleet [54]. The Tesla vehicle batteries come in various configurations between 50-110kWh whereas the Leaf has a 40 kWh battery and the Bolt has a 60kWh [49]. Therefore, the electric vehicle population was chosen to be a distribution of 40, 60, 75, and 100 kWh vehicles with more weight on the medium range. The selected population of vehicles can be seen in Fig. 3.6.

Electric Vehicle Charging Current

The vehicles are assumed to all use a Level 2 or equivalent charger at 240V. The average power that these chargers draw is around 7 kW [49]. However, for more powerful chargers such as the Tesla Wall Connector, the charging current can get as high as 80A which draws 19.2 kW [55]. For the simulation, the current maximum for each electric vehicle is correlated to the vehicle's battery size with an added Beta Distribution (see Fig. 3.6). This is a realistic assumption as owners of vehicle's with a large battery would be more likely to buy a more powerful charger or have a Tesla
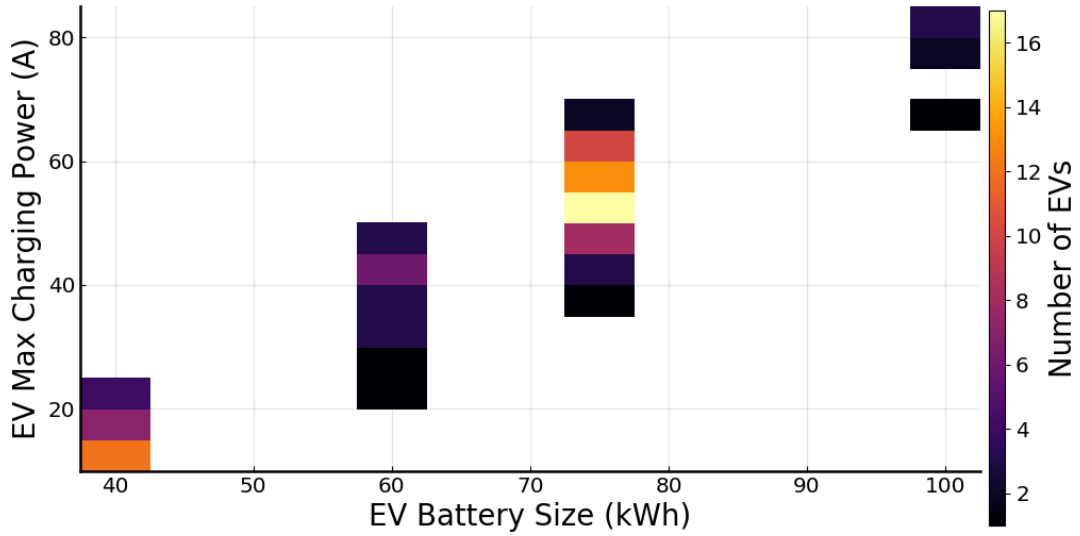
Figure 3.6: Battery Size and Maximum Charging Power

with a Tesla Wall Connector.

Electric Vehicle Schedules

All vehicles are assumed to be available to charge when the simulation begins at 8 PM. The starting state of charge for each vehicle ($S_{\mathrm{meas},n}$) is drawn from a Beta distribution that puts the mean at 40% and the maximum at 70% which can be seen in Fig. 3.7 (a).

$$S_{\mathrm{meas},n} \sim 0.7 * \mathrm{Beta(4,3)} \tag{3.47}$$

The vehicles are assumed to have a departure time between 6:30 AM and 10:00 AM with a minimum state of charge between 75% and 100%. These are drawn from Beta distributions and the values can be seen in Fig. 3.7 (b).

Note: For this simulation, the vehicle do not actual leave at the departure time so they may continue to charge.
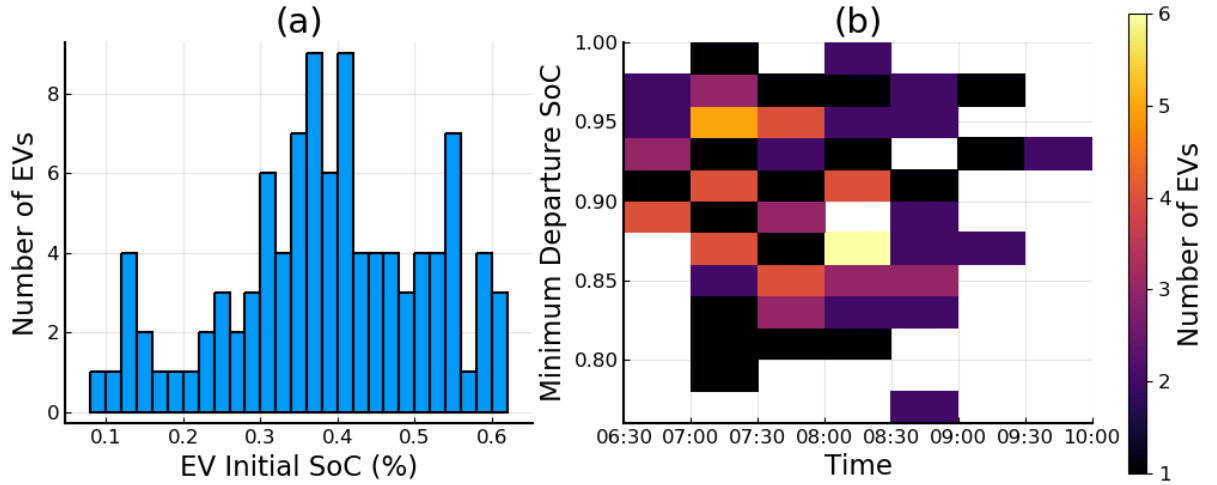
Figure 3.7: Initial SoC (a) and EV Departure Requirements (b)

Objective Weights

The objective weights Q_n and R_n are scaled so the objective terms are approximately the same and then given a uniform distribution.

Summary of Scenario Parameters

Tables 3.1, 3.2, and 3.3 show a summary of the scenario parameters that have been defined above. These parameters describe the system knowns (Table 3.1), transformer parameters (Table 3.2), and EV vehicle parameters (Table 3.3) that are used in the optimization equations.

Table 3.1: Summary of Simulation System Parameters

N	$\tilde{T}_a$	i_d	K	Δt	M
100	[27,30]°C	[3,20]kVA	160	180s	6

Table 3.2: Summary of Transformer Specific Parameters

$T^{\max}$	$I^{\max}$	T_{meas}	γ	τ	ρ	c
120°C	25kA	55°C	0.0131	0.9145	0.0855	29.87

Table 3.3: Summary of EV Specific Parameters

$s_{\text{meas},n}$	$i_n^{\max}$	α_n	β_n	$\bar{s}_n$	$\bar{k}_n$	Q_n	R_n
[0,0.7]	[12,80]A	[80,90]%	[40,100]kWh	[0.75,1]	[210,280]	$[10^3, 2*10^4]$	10^6

3.6.2 Simulation Implementation

The open loop PWL problem is ran in a receding-horizon model predictive control method for the simulations as seen in Fig. 3.8. The iterative approaches are limited by the time step length of 3 minutes to converge to an optimal solution.
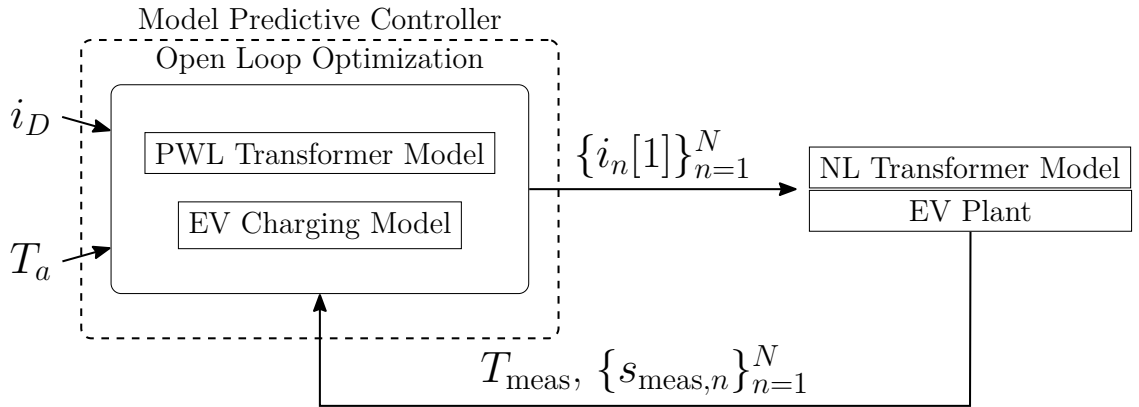
Figure 3.8: Simulation Block Diagram
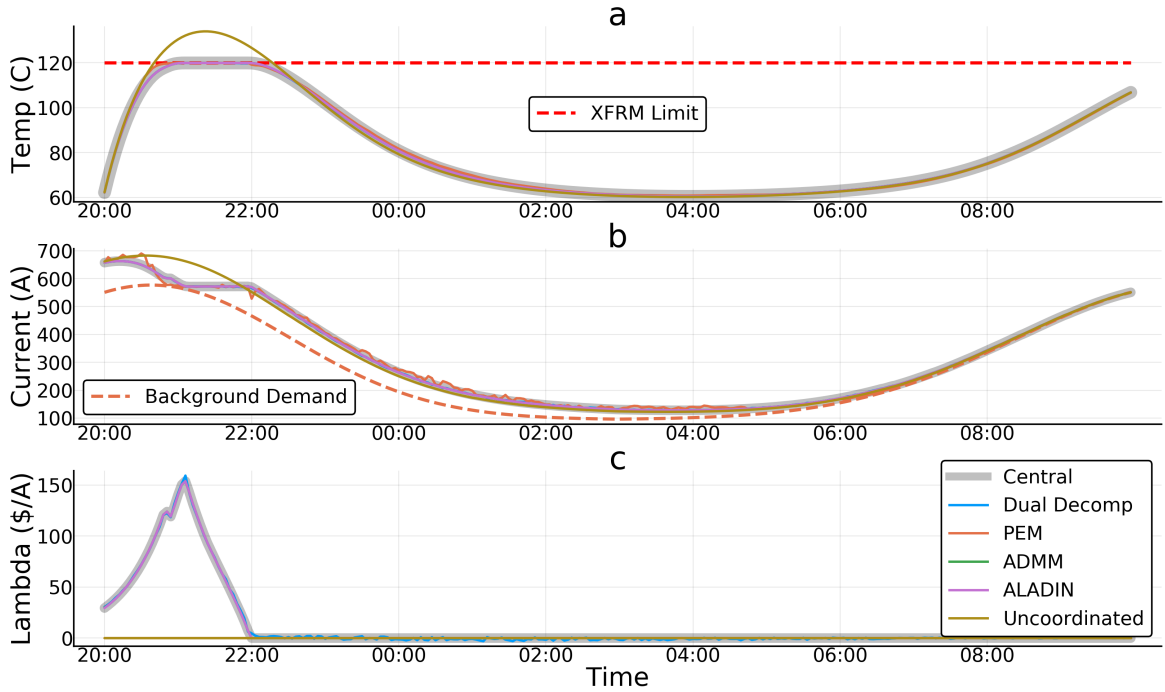
Figure 3.9: Case Study 1 MPC Simulation Results

3.6.3 SIMULATION RESULTS

The closed-loop solution of the MPC simulation for each algorithm as well as the centralized simulation can be seen in Fig. 3.9. The first two graphs show the transformer temperature (a) and total load at the transformer (b). The third (c) should the dual multiplier λ which is associated with the coupling constraint (3.23). In addition to the central solution and the solutions from the four distributed algorithms, the result of the uncoordinated EV charging is plotted. If no EV charging control is implemented, the transformer temperature exceeds the limit.

The optimal solutions of ADMM and ALADIN are nearly identical to the central optimal solution. An example comparison of the convergence between the algorithms for the first time step of the MPC simulation is shown in Fig. 3.10. The first graph
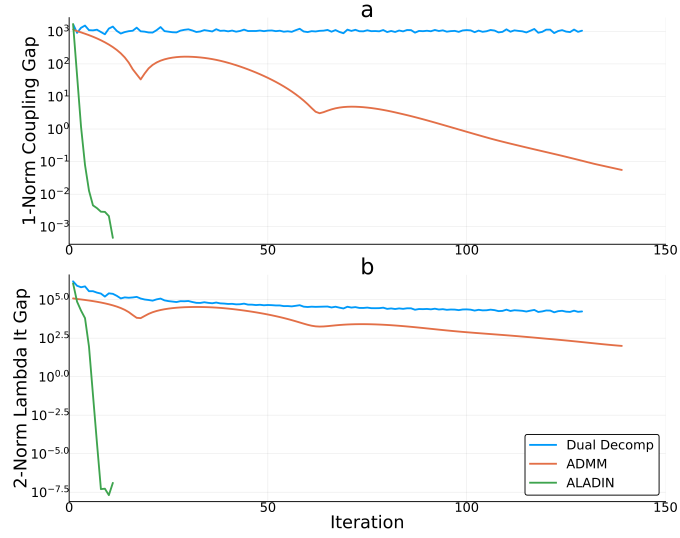
Figure 3.10: Case Study 1 Convergence Cold Start

(a) shows the 1 norm of the coupling constraint at the pth iteration

$$||\mathbf{i}_d + \sum_{n=1}^{N} \mathbf{i}_n^{(p)} - \sum_{m=1}^{M} (\mathbf{i}_m^{PW})^{(p)}||_1 \tag{3.48}$$

and the second graph (b) is the 2 norm of the difference in λ between two iterations

$$||\lambda^{(p)} - \lambda^{(p-1)}||_2 \tag{3.49}$$

The vast performance superiority of ALADIN can be seen while ADMM outperforms Dual Decomposition in both metrics.

42

3.7 Further Analysis

3.7.1 Comparing Nonlinear and PWL Implementations
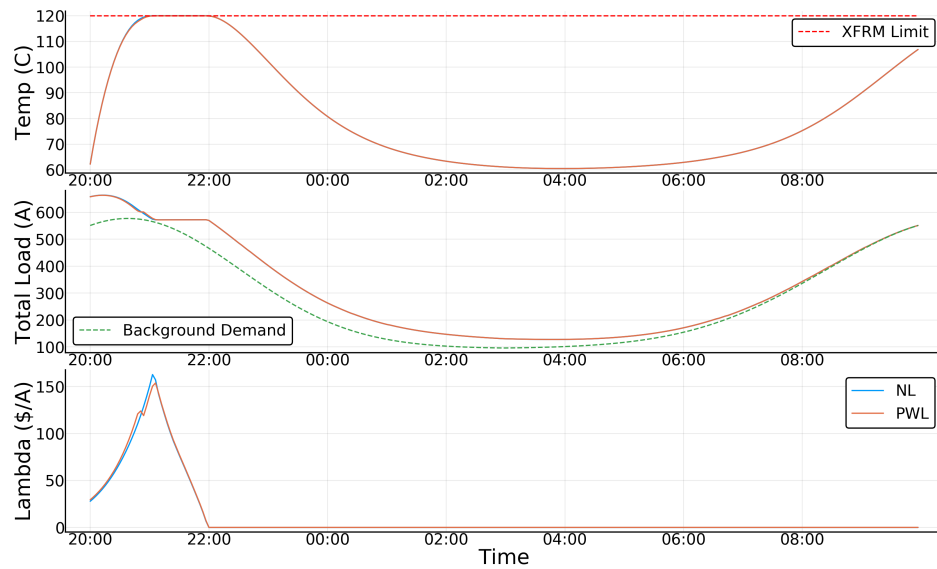
Figure 3.11: NL and PWL central simulation results

In order to justify and verify the use of the PWL relaxation, we compared the solution of the central NL and PWL simulations. In Fig. 3.11, the simulation solutions can be seen to be very similar. However, the difference in computation time is quite different with full MPC simulation of the NL implementation taking 62.8 minutes while the PWL implementation only takes 2.4 minutes. Further verification comes from looking at the solution space of the PWL approximation of the total current as seen in Fig. 3.12. The red dots on the plot are the PWL representation of the square of the total current seen by the transformer before the last timestep of the temperature
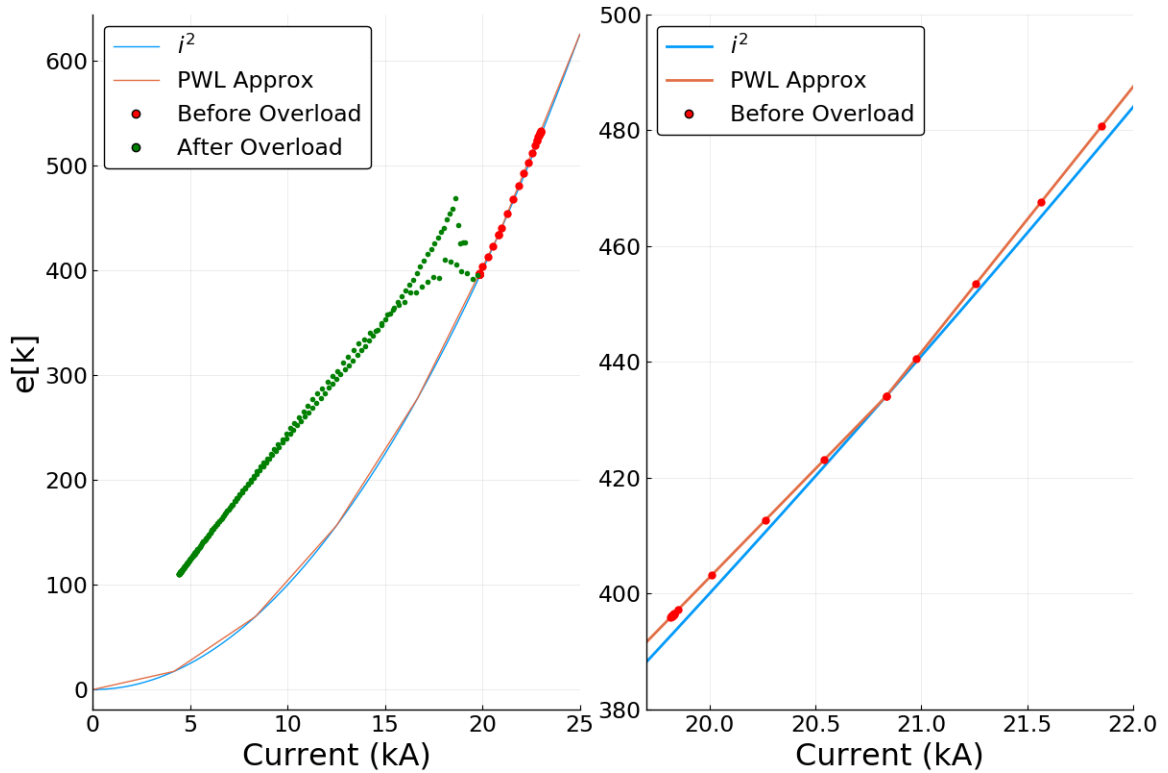
Figure 3.12: PWL Solution Space

limit. On the right side, focusing on these shows that they lie on the PWL segments. The green dots represent the square of the total current after the transformer is overloaded where the fictitious losses are of no importance per Theorem 3.3.1.

3.7.2 Dual Decomposition: Fast Ascent

We develop a modification of the classic dual decomposition to eliminate the transformer problem and speed up the convergence. Examining the transformer problem in Algorithm 1, we can see that it is essentially a feasibly problem. The goal of the transformer is to decide if there exists a sequence of transformer loadings that ensures the temperature stays below the limit. We replace this optimization problem

by estimating the temperature using the local EV schedules and comparing to the temperature limit which is seen in Algorithm 5. The Fast Ascent algorithm increases computational speed and algorithm convergence but has no convergence guarantees.

Algorithm 5 Fast Ascent

Initialization: Initial guess of dual multiplier $\lambda^{(1)}$
Repeat: for $p <$ Max Iterations:

   1. *Local EV Problem:* Solve for each $n \in N$

$$\mathbf{i}_n^{(p)} = \arg\min_{\mathbf{i}_n} \quad J_n(\mathbf{i}_n, \mathbf{s}_n) + (\lambda^{(p)})^T \mathbf{i}_n \tag{3.50}$$

$$\text{s.t.} \quad (3.13\text{f}), (3.13\text{g}), (3.13\text{h})$$

   2. *Coordinator Problem:*

$$T^{(p)}[k+1] = \tau T^{(p)}[k] + \gamma(\sum_{n=1}^{N} i_n^{(p)}[k] + i_D[k])^2 + \rho T_a[k] \quad \forall k = 0, K-1 \tag{3.51}$$

$$\nabla_\lambda \mathcal{L} = \mathbf{T}^{(p)} - T^{\max} \mathbf{1}_K \tag{3.52}$$

$$\lambda^{(p+1)} = \lambda^{(p)} + \alpha^{(p)} \nabla_\lambda \mathcal{L} \tag{3.53}$$

3.7.3 ALADIN: COMPARING INEQUALITY AND EQUALITY FORMULATIONS

As mentioned in Section 3.5.3, the ALADIN algorithm was modified slightly to use inequalities in the coordinator problem. Although this slows the time per iteration down slightly, it enables the coordinator more flexibility to move the variables each iteration which decreases the number of iterations needed to converge. This convergence improvement can be seen in Fig. 3.13.

Complementary to the improved convergence, the inequality implementation of ALADIN has a decrease in computation speed. The equality implementation of AL-
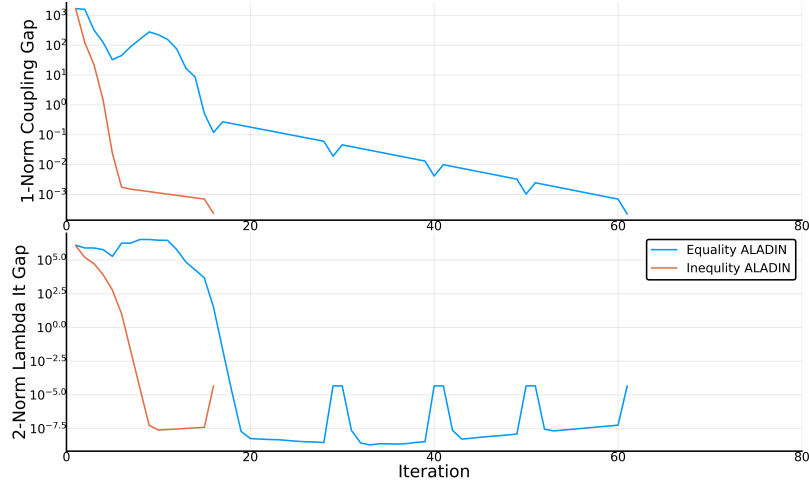
Figure 3.13: Inequality and Equality ALADIN Convergence Comparison

ADIN takes 1.6 hours to run the full MPC simulation while the inequality implementation takes about half as long.

3.7.4   ALADIN: PROTECTING INFORMATION

ALADIN converges very quickly to a solution numerically close to the central solution. However, the tradeoff for this convergence is the magnitude of information and the lack of privacy that comes with it. An option to increase the protection of information is to add some random noise to some of the communicated information.

One of the sets of information that is used in the coordinator problem is the Hessian of the local variables $\{s_n, i_n\}$. In practice, this represents the owners $\frac{Q}{R}$ ratio that they set to determine the tradeoff between reaching full charge and minimizing battery wear. By introducing a small amount of random noise to these Hessians the controller would not know the exact parameters chosen. This would increase the privacy of the ALADIN algorithm but decrease the performance slightly. However, the

46

$\frac{Q}{R}$ ratio is definitely not the most confidential information being sent as the gradients contain the current charging schedules. Adding noise to the gradients would increase the privacy more significantly but the performance would also drop quite a bit.

3.7.5   PEM: Optimizing Performance

There are three main parameters in the Packetized Energy Management scheme seen in Section 3.5.4, the packet length (δ), the mean time to request ($mmtr$), and the ratio set point ($\hat{r}_{set,n}$). By varying these parameters we can attempt to optimize the packetized scheme close to the central optimization solution.
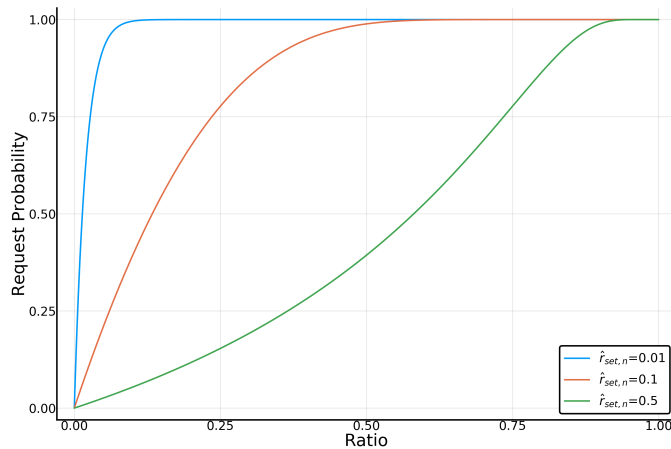
Figure 3.14: Probability of Request as a function of the ratio equation seen in 4 for different values of $\hat{r}_{set,n}$

The PEM scheme performs well when the packet length and mean time to request are similar. This makes intuitive sense as a long packet length and short MTTR would result in over requesting and short packet lengths with a long MTTR would result in under requesting. By looking at equation (13),we can see that changing $mmtr$ and $\hat{r}_{set,n}$ will have similar affects. Therefore for the purpose of this analysis the mean

time to request is help constant at $mttr = \Delta t * \delta$ and $\hat{r}_{\text{set},n}$ is varied. Fig. 3.14 shows the affect of varying the set point for SoC: as $\hat{r}_{\text{set},n}$ is increased the probability of requesting decreases.
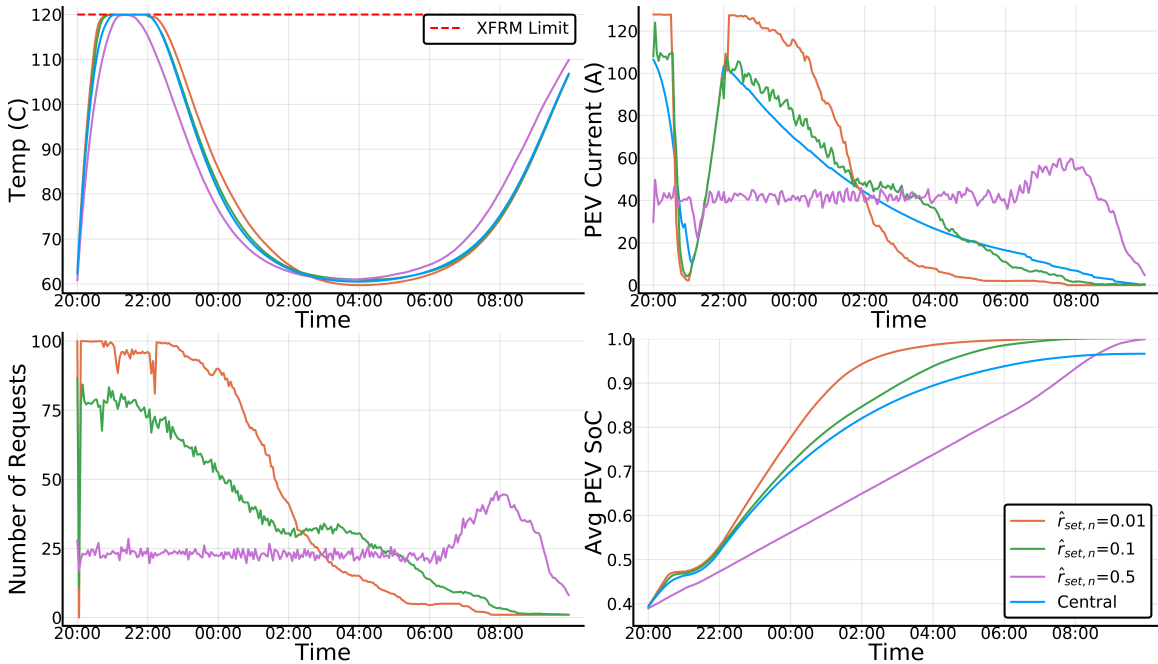
Figure 3.15: Full Analysis of $\hat{r}_{set,n}$ affect on PEM performance

A more comprehensive view in the impact of the set SoC can be seen in Fig. 3.15 where 10 simulations for each selection of $\hat{r}_{\text{set},n}$ were averaged. The simulations with a low value of $\hat{r}_{\text{set},n}$ request more often at the beginning which results in higher currents and the transformer temperature being at its limit for longer. Conversely, a scheme with a high value of $\hat{r}_{\text{set},n}$ requests less often on average and has to charge extra at the end. This might seem preferable at first but with a $\hat{r}_{\text{set},n}$ parameter too high, there is the risk that the PEM algorithm will no longer be able to meet the transformer temperature limits. This can be attributed to "bad planning" as the vehicles do not request enough earlier and end up being forced to opt on. A value

48

in the middle balances requesting frequently enough to give some flexibility where needed and minimizing the communication burden and expenses with more requests. We found $\hat{r}_{\text{set},n} = 0.1$ to fit this need and match closely with the central optimization solution. It is worth noting that PEM has no mechanism to limit the current and battery wear of the vehicles so is not truly trying to solve the same problem as the optimization.

3.7.6 UTILITY FOCUSED OPTIMIZATION

As mentioned in Section 2.3, there are many possible objectives when scheduling the charging of electric vehicles. Thus far the objective of the optimization problem has been focused on the electric vehicle owner and meeting their needs. An additional objective term as a function of the temperature can be added to potentially meet the desire of a distributed grid operator.

$$\sum_{k=1}^{K} \psi_k (T^{\text{max}} - T[k]) \tag{3.54}$$

with $\psi_k < 0$.

Utilities would be able to tune the ψ_k parameter based on how valuable maximizing the distance that the transformer temperature is from its limit. As ψ_k increases the objective problem shifts from a consumer-centric to a valley-filling approach. The results of such a change can be observed in Fig. 3.16. An addition benefit of this augmentation is that the KKT conditions of the convex relaxation are always tight to the nonlinear constraint.
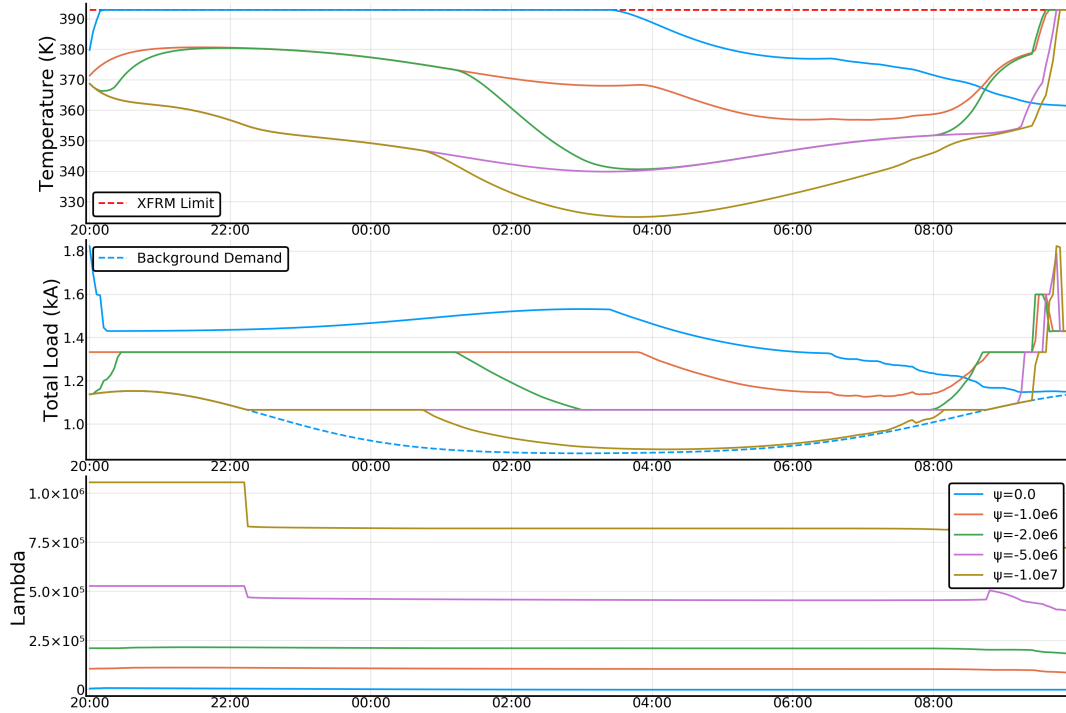
Figure 3.16: Affect of ψ on Optimal Solution

3.7.7 ALGORITHM RESILIENCE: FORECAST ERROR

The problem formulation relies on numerous predicted values including the background demand and ambient temperature. Ambient temperature is a relatively accurately predicted value over the 8-hour MPC prediction horizon and any deviations will be small. While predictions for background demand on a grid operator level are relatively accurate and reliable, the predictions for a distribution network is much more likely to be erroneous due to a smaller portfolio effect. In order to be confident that these algorithms could be resilient in the real world, we need to add some prediction error to our simulations.

Fig. 3.17 shows the comparison with a central simulation with no forecast error
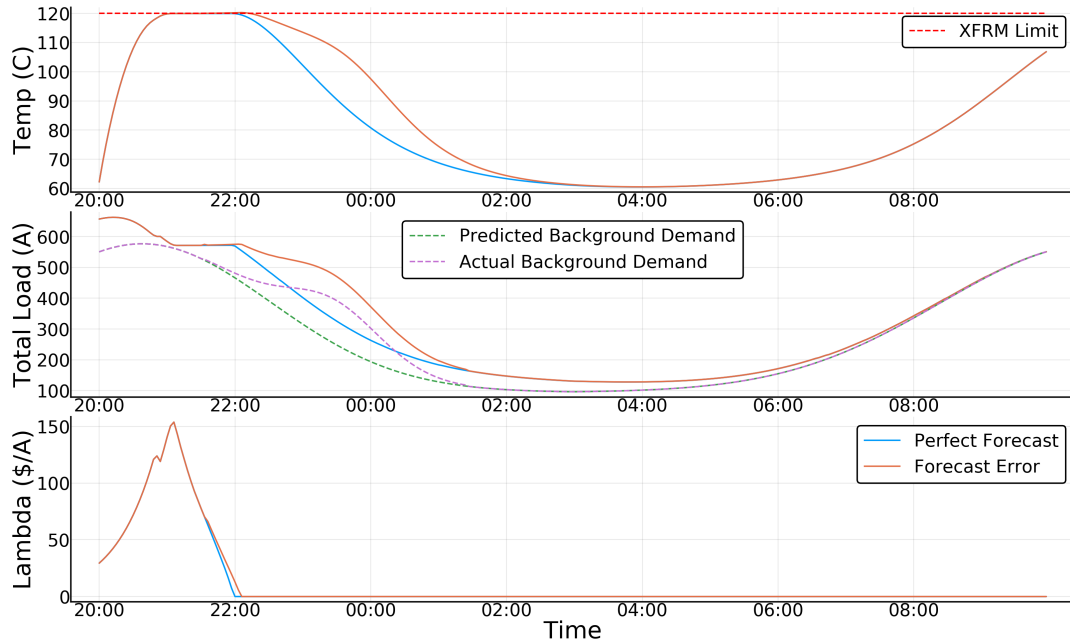
Figure 3.17: Effect of Demand Forecast Error

and one with forecast error between 10 PM and 2 AM. The actual background demand turned out to be much higher than predicted which resulted in the transformer temperature being at the limit for longer and the dual variable being nonzero for longer.

3.7.8 Economic Incentives

Due to the structure of the electricity grid and open access to power, the only way a scheme like this would be implemented in residential areas would be through an opt-in program. In order to get people to sign up, there would need to be some sort of incentive as they are giving up the option to charge whenever they would like. The incentive could come as a societal one for preventing grid overloads or a monetary one.
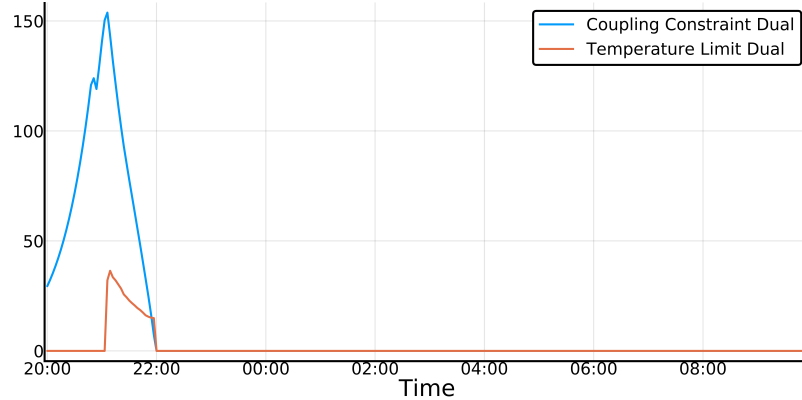
Figure 3.18: Dual Variable Comparison

One option for how a monetary incentive could work would be utilities offering customers a payment based on their calculated cost avoided. By utilizing one of these control algorithms they would reduce the frequency and magnitude of transformer overloads. This would result in a longer lifespan for the transformers and a reduction of costs for the utility. The utility could pass on some of these avoided costs to consumers who enrolled in the program.

Another structure to a monetary incentive could be using the dual variables from the EV charging problem to price the electricity. In the optimization problem there are dual variables associated with the coupling equality constraint (3.23) and the upper temperature limit (3.13e) which could be used as a pseudo real-time price of electricity. The dual variable of the optimal power flow problem is often used in wholesale electricity markets as the locational margin price [56]. A comparison between the two dual variables in the simulation is shown in Fig. 3.18. The dual variable associated with the temperature limit is only positive when the constraint is tight (i.e $T[k] = T^{\mathrm{max}}$). However, the coupling constraint, in this case, is positive for time steps before the overload and peaks at the first tight temperature time step.

This is a favorable price signal to use as it would incentivize EV owners to reduce charging in the time steps as the temperature approaches its limits. A potential program could offer consumers a lower normal electricity rate but subject them to these pseudo real-time rates when the transformers were nearing their limit.

Chapter 4

Hub Charging Problem

In this chapter, we will introduce and motivate a new charging problem that is centered on the idea of charging an electric vehicle hub rather than charging individual vehicles. We will formulate the problem and run simulations for the four distributed algorithms used in Chapter 3.

4.1 Motivation

The residential EV optimal charging problem presented in Section 3 is just one scenario where coordinating the demand related to EV charging will be useful. As commercial transportation becomes electrified, these vehicle fleets will also benefit from scheduled charging control. In addition, a large proportion of these fleets have predictable routes to and from a central warehouse or shipping facility. These central facilities or "hubs" represents centers for electric vehicle charging while vehicles return from completed routes or park overnight.

The commercial/industrial EV hub charging problem is inherently different from

the residential charging problem. For example, the privacy of an individual vehicle in a commercial fleet is not a concern as one company owns and controls all the vehicles in the fleet. The vehicles most likely have larger batteries and since there are multiple electric vehicles in the hub, each hub node represents a much larger total demand on the system than the individual residential EV node in case study 1.

In the formulation below, we represent each hub as a single node in the system and assume that internal to each hub is an algorithm, such as PEM, that distributes charging capacity to individual vehicles. The hub node aggregates available EV states of charge and energy limits to ensure that the hub can meet the underlying EV charging needs. Next, we develop the dynamic model of a hub and the distributed charging control policy to charging EVs in each hub.

4.2   FORMULATION
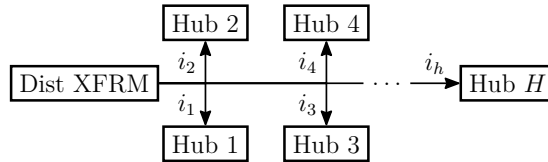
Figure 4.1: Case Study 2 System Schematic

Define H hubs where each has N_h vehicles. Each vehicle is predicted to arrive at time step $\underline{K}_{h,n}$ with arrival energy $\underline{s}_{h,n} E_{h,n}^{\max}$ and it is predicted to leave at time step $\bar{K}_{h,n}$ with desired minimum departure energy $\bar{s}_{h,n} E_{h,n}^{\max}$. The value $E_{h,n}^{\max}$ represents the absolute battery capacity of vehicle n of hub h while the relative SoC at arrival/departure is given by $\underline{s}_{h,n}/\bar{s}_{h,n}$. For each hub and each time-step, we can then

define three dynamic sets for parked, departing, and arriving vehicles:

$$\text{Parked}_h[k] = \{n \in N_h | \underline{K}_{h,n} < k < \bar{K}_{h,n}\} \tag{4.1}$$

$$\text{Depart}_h[k] = \{n \in N_h | k = \bar{K}_{h,n}\} \tag{4.2}$$

$$\text{Arrive}_h[k] = \{n \in N_h | k = \underline{K}_{h,n}\}. \tag{4.3}$$

From the arrival and departure sets above, we can calculate the departure and arrival energy trajectories:

$$E_{h,\text{depart}}[k] = \sum_{n \in \text{Depart}_h[k]} \bar{s}_{h,n} E_{h,n}^{\text{max}} \tag{4.4}$$

$$E_{h,\text{arrive}}[k] = \sum_{n \in \text{Arrive}_h[k]} \underline{s}_{h,n} E_{h,n}^{\text{max}}. \tag{4.5}$$

These trajectories define the amount of energy added and subtracted from the predicted vehicle arrivals and departures, respectively. From the parked vehicles in hub h at time k, we can also define the time-varying upper limits on energy and effective current:

$$E_h^{\text{max}}[k] = \sum_{n \in \text{Parked}_h[k]} E_{h,n}^{\text{max}} \tag{4.6}$$

$$i_h^{\text{max}}[k] = \sum_{n \in \text{Parked}_h[k]} i_{h,n}^{\text{max}}. \tag{4.7}$$

Note that although physically the maximum current of the charging facility would not change, the effective maximum current at k is a function of the number of vehicles that are parked.

Finally, since vehicle n can depart from a hub h with more than its desired de-

parture SoC $\bar{s}_{h,n} E_{h,n}^{\max}$, we need to account for the difference between the expected departing SoC and actually departing with up to 100% of SoC:

$$E_{h,\Delta}^{\max}[k] = \sum_{n \in \text{Depart}_h[k]} (1 - \bar{s}_{h,n}) E_{h,n}^{\max} \tag{4.8}$$

From these sets and trajectories, we can now form the hub energy dynamics.

4.2.1 HUB ENERGY DYNAMICS

The aggregated SoC for each hub at time $k + 1$ is a function of the current delivered over time-step k, the expected energy lost from departing vehicles, and the expected energy gained from arriving vehicles. The departed energy from each time step is the expected target SoC for the departing vehicles plus any extra energy provided, $E_{h,\text{depart}} + E_{h,\Delta}$, which models any extra energy provided to the hub to bring (some) vehicles above their $\bar{s}_{h,n}$ requirement and closer to the 100% SoC.

$$E_h[k + 1] = E_h[k] + \eta_h i_h[k] + E_{h,\text{arrive}}[k] -$$
$$(E_{h,\text{depart}}[k] + E_{h,\Delta}[k]) \tag{4.9}$$
$$0 \leq E_h[k] \leq E_h^{max}[k] \tag{4.10}$$
$$0 \leq E_{h,\Delta}[k] \leq E_{h,\Delta}^{max}[k] \tag{4.11}$$
$$0 \leq i_h[k] \leq i_h^{\max}[k] \tag{4.12}$$

Remark. *Note that the hub charging efficiency η_h is assumed to be time-invariant (i.e., all vehicles charge with the same efficiency). However, hub charging efficiency could be a time-varying parameter and based on a weighted combination of the effi-*

ciencies of all vehicles in $Parked_h[k]$.

Next, we present the subtle differences between the hub system and residential charging problems as it relates to the hub objective function.

4.2.2 OBJECTIVE FUNCTION

The local hub objective function is similar to the one in the local (residential) EV scenario. However, now we want to minimize the deviation of the predicted hub energy level to its maximum possible energy state, which is the sum of the energy capacities for all vehicles forecasted to be parked at their respective hubs. In addition, if it is possible, it is desirable to maximize the $E_{h,\Delta}$ terms as they allow the hub to maximizing the underlying EV SoC. The weighting factor O_h determines how desirable oversupplying energy is relative to the weights of the other two terms (Q_h and R_h), which could be time-dependent.

$$J_h(\mathbf{i}_h, \mathbf{E}_h, \mathbf{E}_{h,\Delta}) = \sum_{k=1}^{K} (E_h[k] - E_h^{\max}[k])^2 Q_h + \tag{4.13}$$
$$(i_h[k])^2 R_h - O_h E_{h,\Delta}[k]$$

The objective function for all hubs is then

$$\min \sum_{h=1}^{H} J_h(\mathbf{i}_h, \mathbf{E}_h, \mathbf{E}_{h,\Delta}). \tag{4.14}$$

58

4.2.3 CENTRAL PWL MODEL

Combining these equations with the same PWL transformer dynamics gives us a centralized control problem for scheduling the current to each hub.

$$\min \ \sum_{h=1}^{H} J_h(\mathbf{i}_h, \mathbf{E}_h, \mathbf{E}_{h,\Delta}) \tag{4.15a}$$

s.t.

$$E_h[k+1] = E_h[k] + \eta_h i_h[k] + E_{h,\text{arrive}}[k] - (E_{h,\text{depart}}[k] + E_{h,\Delta}[k]) \tag{4.15b}$$

$$T[k+1] = \tau T[k] + \rho T_a[k] + \gamma \left(\Delta i \sum_{m=1}^{M} (2m-1) i_m^{PW}[k] \right) \tag{4.15c}$$

$$i_d[k] + \sum_{h=1}^{H} i_h[k] = \sum_{m=1}^{M} i_m^{PW}[k] \quad | \ \lambda[k] \tag{4.15d}$$

$$0 \leq E_h[k] \leq E_h^{\max}[k] \tag{4.15e}$$

$$0 \leq E_{h,\Delta}[k] \leq E_{h,\Delta}^{\max}[k] \tag{4.15f}$$

$$0 \leq i_m^{PW}[k] \leq \Delta i \quad \forall m = 1, \ldots, M \tag{4.15g}$$

$$0 \leq i_h[k] \leq i_h^{\max}[k] \tag{4.15h}$$

$$T[k+1] \leq T^{\max} \tag{4.15i}$$

for all $k = 0, \ldots, K - 1$ and $h = 1, \ldots, H$.

4.2.4 Distributed Hub Model

A similar dual decomposition method can be used by forming the partial Lagrangian

$$\mathcal{L}(\mathbf{i}_h, \mathbf{E}_h, \mathbf{i}_m^{PW}, \lambda) = \sum_{h=1}^{H} J_h(\mathbf{i}_h, \mathbf{E}_h) + \lambda^T \left(\mathbf{i}_d + \sum_{h=1}^{H} \mathbf{i}_h - \sum_{m=1}^{M} \mathbf{i}_m^{PW} \right) \tag{4.16}$$

$$= \sum_{h=1}^{H} \left(J_h(\mathbf{i}_h, \mathbf{E}_h) + \lambda^T \mathbf{i}_h \right) + \lambda^T (\mathbf{i}_d - \sum_{m=1}^{M} \mathbf{i}_m^{PW})) \tag{4.17}$$

4.3 Simulations and Results

4.3.1 Hub Scenario

The hub charging scenario that was simulated is similar to the scenario setup in Section 3.6.1 with a few key difference. We start by assuming that the hubs are in a more industrial or commercial neighborhood and are supported by a three-phase 100MVA distribution-level substation transformer. The low end of this transformer is 13.2kV and local pad mounted transformer take this to 480V. For simplicity, there is assumed to be a constant 40MW inflexible background demand seen in 24 hour industrial parks.

We assume that there are four charging hubs that will serve as our system nodes and that there are 100 electric vehicles at each node. Since this problem concerns larger vehicles such as delivery trucks or buses, the electric vehicle parameters are different as well. The 100 vehicles are drawn from a distribution of 100, 200, and 600 kWh that have the ability to charge between 10 and 35 kW. This assumption is reasonable as commerical vehicle will have bigger battery sizes and commercial

60

buildings supported by 480V can handle larger charging powers.

There is assumed to be no vehicles parked at 8 PM when the simulation start and they all arrive with uniform distribution before 10 PM. When they park they have between 0-20 % SoC left since their routes will be more predictable and optimized than the average private electric vehicle owner. The vehicles need to leave between 6 AM and 10 AM and require between 80-100% SoC when they depart. Unlike Case Study 1, the model incorporates the vehicles arriving and leaving which is captured in the changes in $E_h^{\max}$ and $i_h^{\max}$.

4.3.2 Hub Charging Simulation
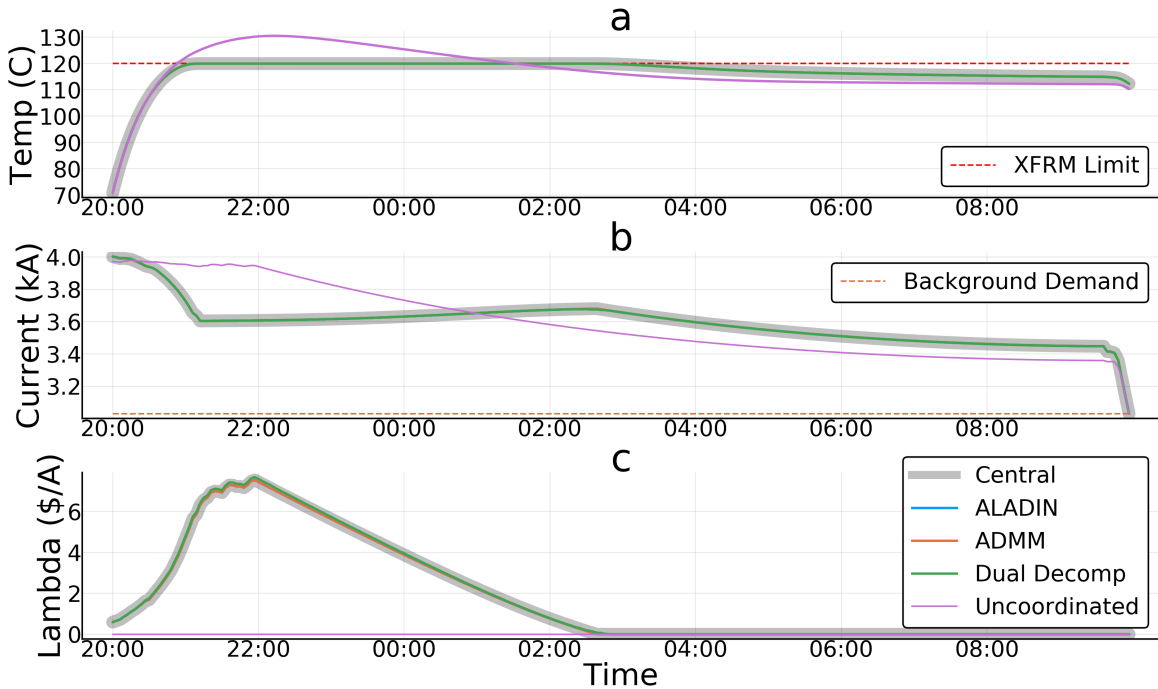
Figure 4.2: Hub Charging Problem Distributed Solutions

The central and uncoordinated results can be seen compared with the optimization

algorithms solutions in Fig. 4.2. Once again, ALADIN and ADMM perform very well and match the central solution to a reasonable accuracy. Here Dual Decompostion performs poorly and can be seen oscillating.

Packetized energy management is less suited for coordinating the charging of the hubs. Since the packetized scheme allows for only boolean states of charging and the hub represents 100 EVs the difference between accepting a packet and rejecting a packet has a significant impact on the transformer temperature. Seen in Fig. 4.3 is the attempt of PEM to coordinate the hub charging. In the beginning, it does a decent job of alternating packets. However, although it continues to receive packet requests as seen in Fig. 4.3 (d) it reaches a state where it cannot accept another packet without overloading the transformer. It continues in this holding pattern until the hubs opt-on and forces a transformer overload which can be seen in the high spikes in current and temperature in Fig. 4.3 (b) and (c).
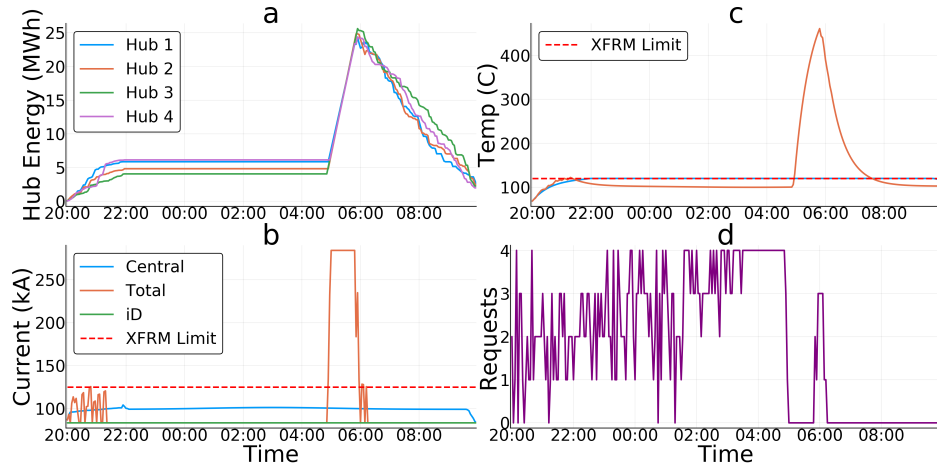
Figure 4.3: Hub Charging Problem PEM

Due to its extremely quick convergence, ALADIN may be an ideal approach for solving control problems where privacy is less important as in this case study.

62

Chapter 5

Comparison of Distributed Methods

In this chapter, we compare the results of the two Case Studies across the four distributed algorithms. First, we look specifically at each assessment metric: privacy, performance, and processing speed. Then, we give a more qualitative summary and discussion on the tradeoffs between distributed methods.

5.1 Privacy and Communication

Table 5.1 shows the information communicated between the EVs, Coordinator, and Transformer. The most valuable information from a consumer standpoint is the current and SoC schedules. While both Dual Ascent and ADMM transfer the current schedule to the coordinator, the coordinator only uses the sum of the current schedules so this sensitive information could be passed through a third party and aggregated first. However, in ALADIN the current schedule is used in the coordinator problem

as well as in the gradient.

Table 5.1: Information Sharing of Distributed Methods

	ALADIN	ADMM	Dual Decomp	PEM
EV to Coordinator	$\mathbf{i}_n^{(p)}$, $\mathbf{g}_{i,n}^{(p)}$, $\mathbf{g}_{s,n}^{(p)}$, $\mathbf{C}_{\bar{i},n}^{(p)}$, $\mathbf{C}_{\underline{i},n}^{(p)}$, $\mathbf{C}_{\bar{s},n}^{(p)}$, $\mathbf{C}_{\underline{s},n}^{(p)}$	$\mathbf{i}_n^{(p)}$	$\mathbf{i}_n^{(p)}$	$Req_n[k]$
Transformer to Coordinator	$\sum_{m=1}^{M}(\mathbf{i}_m^{PW})^{(p)}$, $\mathbf{g}_{i,PW}^{(p)}$, $\mathbf{g}_t^{(p)}$, $\mathbf{C}_{\bar{z}}^{(p)}$, $\mathbf{C}_{\underline{z}}^{(p)}$, $\mathbf{C}_{\bar{t}}^{(p)}$, $\mathbf{C}_{\underline{t}}^{(p)}$	$\sum_{m=1}^{M}(\mathbf{i}_m^{PW})^{(p)}$	$\sum_{m=1}^{M}(\mathbf{i}_m^{PW})^{(p)}$	$T[k]$
Coordinator to EV	$\lambda^{(p)}$, $\mathbf{V}_{i,n}^{(p)}$, $\mathbf{V}_{s,n}^{(p)}$	$\lambda^{(p)}$, $\mathbf{V}_{i,n}^{(p)}$	$\lambda^{(p)}$	$Rec_n[k]$
Coordinator to Transformer	$\lambda^{(p)}$, $\mathbf{V}_t^{(p)}$, $\mathbf{V}_{i,PW}^{(p)}$	$\lambda^{(p)}$, $\mathbf{V}_{i,PW}^{(p)}$	$\lambda^{(p)}$	-

An approximate quantization of the amount of information shared for each time step assuming that the method takes the average number of iterations, $N = 100$, and the horizon length equals 160 is: 2 kilobits per timestep for PEM, 2 gigabits per timestep for Dual Ascent, 330 megabits per timestep for ADMM, and 65 megabits per timestep for ALADIN. Table 5.2 shows the information communicated per device per timestep as well as what percentage this takes of an average US internet connection of 18.7 Megabits per second [57].

Table 5.2: Case Study 1 Communication Overhead of Distributed Methods for Single device

	ALADIN	ADMM	Dual Decomp	PEM
Information per Timestep (bits)	6e5	3e6	2e7	3e1
Percentage of Avg US bandwidth (%)	0.02	0.09	0.6	≈ 0

5.2 PERFORMANCE

A summary of the performance of the four distributed methods in terms of the 2-norm of the current schedules and dual variable between the central and distributed

solution is shown in Table 5.3. Here the 2-norm was used to show the total difference between the distributed method solution and the centralized solution per the following equations:

$$||i_n^* - i_n||_2 \tag{5.1}$$

$$||\lambda^* - \lambda||_2 \tag{5.2}$$

Table 5.3: 2-Norm Distributed Methods Performance

	2-Norm Current Schedule		2-Norm Lambda	
Method	Case Study 1	Case Study 2	Case Study 1	Case Study 2
ALADIN	8e−2	8e−3	1e−3	2e−5
ADMM	1e0	1e1	5e−1	1e−2
Dual Decomposition	7e1	2e2	2e1	9e−1
PEM	3e3	4e5	-	-

The units on i_n are Amperes in this calculation so these can be interpreted as total current difference across all vehicles and time steps. For a different view into the performance gap between the distributed methods and the centralized, we can look at the RMSE for the current schedule and dual variable:

$$\sqrt{\frac{\sum_{n=1}^{N} \sum_{k=1}^{K} (i_n^*[k] - i_n[k])}{NK}} \tag{5.3}$$

$$\sqrt{\frac{\sum_{k=1}^{K} (\lambda^* - \lambda)}{K}} \tag{5.4}$$

The RMSE for the current schedule can be thought of as the average current difference for any time step in Amperes. The values for the current schedule and dual variable λ can be seen in Table 5.4.

In both case studies, ALADIN and ADMM performed well in that their solution

Table 5.4: RMSE Distributed Methods Performance

	RMSE Current Schedule		RMSE Lambda	
Method	Case Study 1	Case Study 2	Case Study 1	Case Study 2
ALADIN	5e−4	2e−4	6e−5	1e−6
ADMM	8e−3	3e−1	3e−2	5e−4
Dual Decomposition	4e−1	2e2	1e0	6e−2
PEM	2e1	1e4	-	-

was very accurate when compared to the central solution. Dual decomposition follows these two but with significantly worse performance. The PEM scheme will never reach the optimal solution and therefore the differences in the current schedules are more pronounced.

5.3   COMPUTATION SPEED

A summary of the computational speed for the methods can be seen in Table 5.5. The first metric tracks how long it takes the algorithm to solve for each time step on average. This number is not necessarily proportional to the average number of iterations shown in the other columns as some algorithms take longer for each iteration. The central and PEM implementations are much faster than any others as they are iterative-free approaches. ALADIN is the next quickest followed by ADMM and Dual Decompostion. In the implementation the algorithms have a constraint on the number of iterations due to the length of the time step. Increasing the number of electric vehicles in the simulation would likely have a similar number of iterations per time step however the performance especially for dual decomposition and ADMM would decrease. It is worth nothing that the stopping criteria and maximum number of iterations was different for Case Study 1 and Case Study 2.

Table 5.5: Summary of Distributed Methods Speed

Method	Sec./Time Step		Average Iter. to Converge	
	Case Study 1	Case Study 2	Case Study 1	Case Study 2
Central	0.7	0.1	1	1
ALADIN	15.5	1.25	7.6	2.2
ADMM	71.7	17.25	73.3	116
Dual Decomposition	150	150	500	3408
PEM	0.15	0.05	1	1

5.4 SUMMARY OF RESULTS

A qualitative summary of the differences in the distributed methods is shown in Fig. 5.1. The central formulation gives the optimal solution quickly but gives no privacy and has a high communication overhead. Dual decomposition and ADMM increase the privacy of the implementation but see a significant decrease in the performance and computational speed. ALADIN shows the best performance out of the distributed methods but sacrifices privacy. PEM is the most unique method with maximum privacy and speed but without any optimal performance guarantees.

5.5 SELECTING THE BEST DISTRIBUTED METHOD

For the scenario in Case Study 1, privacy is very important as residential EV owners will not want to share their information. Using ALADIN, the coordinator knows the gradients which are a scaled version of the current schedule so it has highly sensitive data. Due to the high amount of information being shared with the ALADIN algorithm, this may not be the best approach even though it shows the best performance.

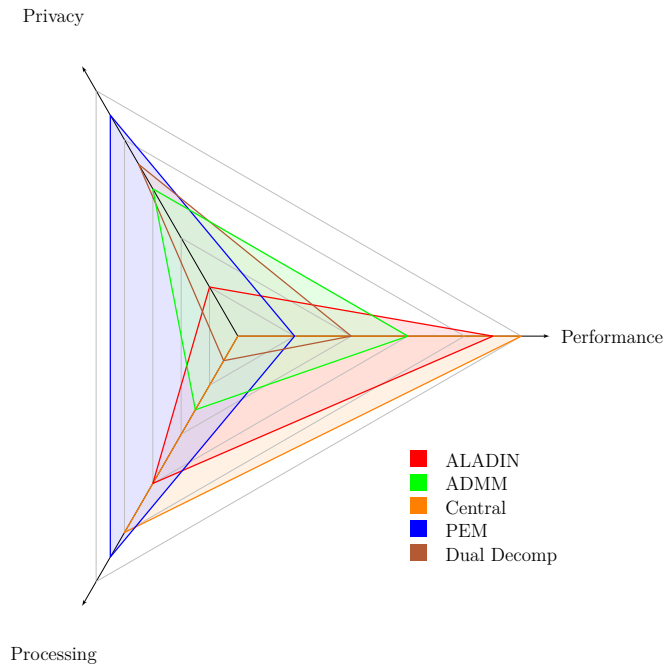*Figure 5.1: Qualitative Comparison of EVC Control Methods*

Depending on how important reaching the optimal solution is, ADMM or PEM could be used for the problem in Case Study 1. For Case Study 2, however, ALADIN is a great fit as the commercial application will likely mean that privacy is less of a priority. It is important to consider the order of priorities before deciding on an algorithm to use for a certain problem.

CHAPTER 6

CONCLUSION AND FUTURE RESEARCH

6.1 CONCLUSION

Utilities and other entities in the energy industry will soon have to consider the impacts of increased adoption of electric vehicles. In this thesis, we looked specifically at how to prevent transformer overloaded by coordinating the charging of electric vehicles. By doing so using a wisely selected distributed control methods we can expand the life of the transformer and prevent costly capital investments while protecting privacy when needed.

We evaluated the ability of four distributed algorithms to prevent overloads and meet the objectives in two case studies. We found that there was a tradeoff between an algorithm's performance, protection of information, and computational speed. For an application where privacy is of paramount importance, such as a residential EV charging problem, we found that a suboptimal but privacy-preserving algorithm such as packetized energy management might be ideal. On the other hand, in a commercial setting, such as the hub charging problem, where performance might take priority a

quick converging algorithm such as ALADIN would be a good choice. By selecting the appropriate distributed algorithm for the problem, we can satisfy the constraints and properly coordinate the charging of electric vehicles.

The main contributions of this thesis and related work are:

- Implementing novel distributed optimization approach, ALADIN, for solving EV charging problem

- Adapting iterative-free coordination scheme, PEM, for solving EV charging problem with dynamic constraints

- Developing electric vehicle hub charging problem

- Comprehensive comparison of tradeoff of distributed methods for solving electric vehicle and hub type problems

6.2 FUTURE RESEARCH

There are numerous aspects of the hub problem that could be improved to make the scenario more realistic. Right now the window of time where vehicles arrive and depart are mutually exclusive. Depending on the company that is managing the vehicle routes, these windows could be overlapping or even have vehicles arriving and departing all 24 hours of the day. Furthermore, there could be a scenario where the company has no well-founded predictions on when the vehicles are arriving or leaving. One realistic application could be an electric bike share or electric car share program. If the vehicle population was small the lack of forecasting would introduce major complications, however, if the population was large enough statistical methods

could be used to predict the probability of vehicles arriving or leaving based on past behavior.

There are also some assumptions that could be expanded to test other scenarios. For example, we assume the background demand is always positive but if there was a high solar penetration this number could go negative. We also assume that the EV current is positive and that the vehicles can not discharge to the grid. It would be worth investigating how adding solar and vehicle to grid scenarios would impact the EV charging simulations. Both the neighborhood electric vehicle problem and the hub problem could be improved by introducing a network and power flow model. This would model the real world applications much more accurately. Finally, more analysis and research could be done about the future of electric vehicles sizes and charging power as well as transformers with the intention of being able to model future grid behaviors.

Bibliography

[1] Michael J. Safoutin, Joseph McDonald, and Ben Ellies. Predicting the future manufacturing cost of batteries for plug-in vehicles for the u.s. environmental protection agency (epa) 2017-2025 light-duty greenhouse gas standards. *World Electric Vehicle Journal*, 9(3), 2018.

[2] Jeremy Hodges. Electric car costs set to fall, Mar 2018. https://www.bloomberg.com/news/articles/2018-03-22/electric-car-costs-set-to-fall.

[3] Department of Energy. Electric car safety, maintenance, and battery life. https://www.energy.gov/eere/electricvehicles/electric-car-safety-maintenance-and-battery-life.

[4] Nicolas Zart. Do electric vehicles have better overall safety? part 2, Apr 2018. https://cleantechnica.com/2018/04/01/do-electric-vehicles-have-better-overall-safety-part-2/.

[5] Damian Carrington. Electric cars already cheaper to own and run than petrol or diesel-study, Dec 2017. https://www.theguardian.com/environment/2017/dec/01/electric-cars-already-cheaper-to-own-and-run-than-petrol-or-diesel-study.

[6] Loren McDonald. 10% of new vehicles purchased in california are evs, Nov 2018. https://cleantechnica.com/2018/11/12/10-of-new-vehicles-purchased-in-california-are-evs/.

[7] Stephen Schey, Don Scoffield, and John Smart. A first look at the impact of electric vehicle charging on the electric grid in the ev project. *World Electric Vehicle Journal*, 5(3):667–678, 2012.

[8] Eric W. Wood, Clement L. Rames, Abdulkadir Bedir, Noel Crisostomo, and Jennifer Allen. California plug-in electric vehicle infrastructure projections: 2017-

2025 - future infrastructure needs for reaching the state's zero emission-vehicle deployment goals. 3 2018.

[9] Eric Schmidt. Ev clustered charging can be problematic for electrical utilities, Mar 2018. https://www.fleetcarma.com/ev-clustered-charging-can-problematic-electrical-utilities/.

[10] A. D. Hilshey, P. D. H. Hines, P. Rezaei, and J. R. Dowds. Estimating the impact of electric vehicle smart charging on distribution transformer aging. *IEEE Transactions on Smart Grid*, 4(2):905–913, June 2013.

[11] D. K. Molzahn, F. DǍśrfler, H. Sandberg, S. H. Low, S. Chakrabarti, R. Baldick, and J. Lavaei. A survey of distributed optimization and control algorithms for electric power systems. *IEEE Transactions on Smart Grid*, 8(6):2941–2962, Nov 2017.

[12] Ralph M. Hermans, Andrej Jokić, Mircea Lazar, Alessandro Alessio, Paul P.J. van den Bosch, Ian A. Hiskens, and Alberto Bemporad. Assessment of non-centralised model predictive control techniques for electrical power networks. *International Journal of Control*, 85(8):1162–1177, 2012.

[13] A. Ghavami, K. Kar, and A. Gupta. Decentralized charging of plug-in electric vehicles with distribution feeder overload control. *IEEE Transactions on Automatic Control*, 61(11):3527–3532, Nov 2016.

[14] Omid Ardakanian, Catherine Rosenberg, and S. Keshav. Distributed control of electric vehicle charging. In *Proceedings of the Fourth International Conference on Future Energy Systems*, e-Energy '13, pages 101–112, New York, NY, USA, 2013. ACM.

[15] O. Ardakanian, S. Keshav, and C. Rosenberg. Real-time distributed control for smart electric vehicle chargers: From a static to a dynamic study. *IEEE Transactions on Smart Grid*, 5(5):2295–2305, Sept 2014.

[16] R. Carli and M. Dotoli. A decentralized control strategy for optimal charging of electric vehicle fleets with congestion management. In *2017 IEEE International Conference on Service Operations and Logistics, and Informatics (SOLI)*, pages 63–67, Sept 2017.

[17] H. Fan, C. Duan, C. Zhang, L. Jiang, C. Mao, and D. Wang. Admm-based multiperiod optimal power flow considering plug-in electric vehicles charging. *IEEE Transactions on Power Systems*, 33(4):3886–3897, July 2018.

[18] X. Zhou, P. Wang, and Z. Gao. Admm-based decentralized charging control of plug-in electric vehicles with coupling constraints in distribution networks. In *2018 37th Chinese Control Conference (CCC)*, pages 2512–2517, July 2018.

[19] R. Carli and M. Dotoli. A decentralized control strategy for optimal charging of electric vehicle fleets with congestion management. In *2017 IEEE International Conference on Service Operations and Logistics, and Informatics (SOLI)*, pages 63–67, Sep. 2017.

[20] J. Rivera, P. Wolfrum, S. Hirche, C. Goebel, and H. Jacobsen. Alternating direction method of multipliers for decentralized electric vehicle charging control. In *52nd IEEE Conference on Decision and Control*, pages 6960–6965, Dec 2013.

[21] W. Ma, V. Gupta, and U. Topcu. On distributed charging control of electric vehicles with power network capacity constraints. In *2014 American Control Conference*, pages 4306–4311, June 2014.

[22] M. Liu, P. K. Phanivong, and D. S. Callaway. Customer-and network-aware decentralized ev charging control. In *2018 Power Systems Computation Conference (PSCC)*, pages 1–7, June 2018.

[23] S. Weckx, R. D'Hulst, B. Claessens, and J. Driesensam. Multiagent charging of electric vehicles respecting distribution transformer loading and voltage limits. *IEEE Transactions on Smart Grid*, 5(6):2857–2867, Nov 2014.

[24] M. Liu, P. K. Phanivong, Y. Shi, and D. S. Callaway. Decentralized charging control of electric vehicles in residential distribution networks. *IEEE Transactions on Control Systems Technology*, 27(1):266–281, Jan 2019.

[25] B. Yang, J. Li, Q. Han, T. He, C. Chen, and X. Guan. Distributed control for charging multiple electric vehicles with overload limitation. *IEEE Transactions on Parallel and Distributed Systems*, 27(12):3441–3454, Dec 2016.

[26] Y. Zhou, R. Kumar, and S. Tang. Incentive-based distributed scheduling of electric vehicle charging under uncertainty. *IEEE Transactions on Power Systems*, 34(1):3–11, Jan 2019.

[27] Z. Ma, D. S. Callaway, and I. A. Hiskens. Decentralized charging control of large populations of plug-in electric vehicles. *IEEE Transactions on Control Systems Technology*, 21(1):67–78, Jan 2013.

[28] L. Gan, U. Topcu, and S. H. Low. Optimal decentralized protocol for electric vehicle charging. *IEEE Transactions on Power Systems*, 28(2):940–951, May 2013.

[29] X. Huang, C. Xu, P. Wang, and H. Liu. Lnsc: A security model for electric vehicle and charging pile management based on blockchain ecosystem. *IEEE Access*, 6:13565–13574, 2018.

[30] Fabian Knirsch, Andreas Unterweger, and Dominik Engel. Privacy-preserving blockchain-based electric vehicle charging with dynamic tariff decisions. *Computer Science - Research and Development*, 33(1):71–79, Feb 2018.

[31] Fatih Yucel, Kemal Akkaya, and Eyuphan Bulut. Efficient and privacy preserving supplier matching for electric vehicle charging. *Ad Hoc Networks*, 2018.

[32] H. Chen, Z. Guo, Y. Xin, Y. Zhao, and Y. Jia. Coordination of pev charging across multiple stations in distribution networks using aggregate pev charging load model. In *2017 International Smart Cities Conference (ISC2)*, pages 1–5, Sept 2017.

[33] Z. Wei, Y. Li, Y. Zhang, and L. Cai. Intelligent parking garage ev charging scheduling considering battery charging characteristic. *IEEE Transactions on Industrial Electronics*, 65(3):2806–2816, March 2018.

[34] Y. Ota, H. Taniguchi, H. Suzuki, J. Baba, and A. Yokoyama. Aggregated storage strategy of electric vehicles combining scheduled charging and v2g. In *ISGT 2014*, pages 1–5, Feb 2014.

[35] A. M. Jenkins, C. Patsios, P. Taylor, O. Olabisi, N. Wade, and P. Blythe. Creating virtual energy storage systems from aggregated smart charging electric vehicles. *CIRED - Open Access Proceedings Journal*, 2017(1):1664–1668, 2017.

[36] S. Izadkhast, P. Garcia-Gonzalez, and P. FrǍas. An aggregate model of plug-in electric vehicles for primary frequency control. In *2016 IEEE Power and Energy Society General Meeting (PESGM)*, pages 1–1, July 2016.

[37] R. Hermans, M. Almassalkhi, and I. Hiskens. Incentive-based coordinated charging control of plug-in electric vehicles at the distribution-transformer level. In *2012 American Control Conference (ACC)*, pages 264–269, June 2012.

[38] B. Houska, J. Frasch, and M. Diehl. An augmented lagrangian based algorithm for distributed nonconvex optimization. *SIAM Journal on Optimization*, 26(2):1101–1127, 2016.

[39] M. Almassalkhi, J. Frolik, and P. Hines. Packetized energy management: Asynchronous and anonymous coordination of thermostatically controlled loads. In *2017 American Control Conference (ACC)*, pages 1431–1437, May 2017.

[40] Ieee guide for loading mineral-oil-immersed transformers and step-voltage regulators. *IEEE Std C57.91-2011 (Revision of IEEE Std C57.91-1995)*, pages 1–123, March 2012.

[41] A. Seier, P. D. H. Hines, and J. Frolik. Data-driven thermal modeling of residential service transformers. *IEEE Transactions on Smart Grid*, 6(2):1019–1025, March 2015.

[42] M. Hong. A distributed, asynchronous, and incremental algorithm for nonconvex optimization: An admm approach. *IEEE Transactions on Control of Network Systems*, 5(3):935–945, Sep. 2018.

[43] S Boyd. Notes on decomposition methods. *Notes for EE364B*, pages 1–36, 01 2007.

[44] Dimitri P. Bertsekas. *Convex optimization algorithms.* Athena Scientific, 2015.

[45] Ieee guide for loading mineral-oil-immersed transformers and step-voltage regulators - redline. *IEEE Std C57.91-2011 (Revision of IEEE Std C57.91-1995) - Redline*, pages 1–172, March 2012.

[46] United States. Bureau of Reclamation. *Permissible Loading of Oil-immersed Transformers and Regulators.* U.S. Department of the Interior, Bureau of Reclamation, 1991.

[47] H. Nordman, N. Rafsback, and D. Susa. Temperature responses to step changes in the load current of power transformers. *IEEE Transactions on Power Delivery*, 18(4):1110–1117, Oct 2003.

[48] M. T. Isha and Z. Wang. Transformer hotspot temperature calculation using ieee loading guide. In *2008 International Conference on Condition Monitoring and Diagnosis*, pages 1017–1020, April 2008.

[49] John Wamburu, Stephen Lee, Prashant Shenoy, and David Irwin. Analyzing distribution transformers at city scale and the impact of evs and storage. pages 157–167, 06 2018.

[50] Danny S Parker. Research highlights from a large scale residential monitoring study in a hot climate. *Energy and Buildings*, 35(9):863 – 876, 2003.

[51] Fereidoun Ahourai, Irvin Huang, and Mohammad Abdullah Al Faruque. Modeling and simulation of the ev charging in a residential distribution power grid. 11 2013.

[52] Justine Sears, David Roberts, and Karen Glitman. A comparison of electric vehicle level 1 and level 2 charging efficiency. pages 255–258, 07 2014.

[53] Nathaniel Kong. Exploring electric vehicle battery charging efficiency, Sep 2018. https://ncst.ucdavis.edu/wp-content/uploads/2018/09/Kong_NCST-Fellowship-Report.pdf.

[54] Monthly plug-in ev sales scorecard: Historical charts. https://insideevs.com/monthly-plug-in-ev-sales-scorecard-historical-charts/.

[55] Wall connector, Mar 2019. https://www.tesla.com/support/home-charging-installation/wall-connector.

[56] T. Orfanogianni and G. Gross. A general formulation for lmp evaluation. *IEEE Transactions on Power Systems*, 22(3):1163–1173, Aug 2007.

[57] A. Technologies. *Akamai State of the Internet / Connectivity Report: Q1 2017*. Gatekeeper Press, 2017.

[58] P. Rezaei, J. Frolik, and P. D. H. Hines. Packetized plug-in electric vehicle charge management. *IEEE Transactions on Smart Grid*, 5(2):642–650, March 2014.

Appendices

A   SOC Proof of Tightness

We are now interested in how the convex relaxation of transformer model behaves at optimality. Specifically, it is important for the transformer model to accurately represent the physics of the transformer. Since the MPC problem embodies a (convex) QP problem with convex constraints, Slater's constraint qualification is satisfied trivially and the KKT conditions, therefore, provide necessary conditions for (global) optimality. Therefore, we need to understand under which conditions, the convex relaxation is tight, which implies a need to examine KKT optimality conditions.

Rewriting the central NL problem with a convex relaxation and in terms of initial temperature and SoC gives the constraints

$$0 = T[k+1] - \tau^k T_{\text{meas}} - \gamma \sum_{l=1}^{k} \tau^{k-l}(e[l])$$

$$- \rho \sum_{l=1}^{k} \tau^{k-l} T_a[l] \tag{6.1a}$$

$$0 \geq i_{\text{total}}[k]^2 - e[k] \tag{6.1b}$$

$$0 = i_{\text{total}}[k] - i_d[k] - \sum_{n=1}^{N} i_n[k] \tag{6.1c}$$

$$0 \geq T[k+1] - T^{\max} \tag{6.1d}$$

Gradient conditions for variable $T[k+1]$ and $e[l]$ for some $l \leq k$ are

$$\nabla_{T[k+1]}\mathcal{L}: \quad 0 = \lambda_T^{k+1} + \overline{\mu}_T^{k+1} \tag{6.2}$$

$$\nabla_{e[l]}\mathcal{L}: \quad 0 = -\mu_e^l - \sum_{t=l}^{l} \beta^t \lambda_T^t \tag{6.3}$$

for a $\beta^t > 0$ and

- $\lambda_T^{l+1} \in \mathbb{R}_+$ multiplier associated with (6.1a)

- $\mu_e^l \in \mathbb{R}_+$ multiplier associated with (6.1b)

- $\overline{\mu}_T^{k+1} \in \mathbb{R}_+$ multiplier associated with (6.1d)

Consider the case when an overload occurs at $k+1$, i.e. $T[k+1] > \overline{T}$, then $\overline{\mu}_T^{k+1} > 0$. It is immediately straightforward to see that $\lambda_T^{k+1} < 0$. Since $\overline{\mu}_T^t \geq 0$ for all t, $\lambda_T^t \leq 0$ for all t. Therefore the sum of all $\beta^t \lambda_T^t$ in (6.3) must be strickly negative which leads us to $\mu_e^l > 0$. Since l was arbitrarily selected it must hold for all $l \leq k$. Hence, the relaxation is tight for all time steps before the overload.

Remark. *Extending proof to other relevant formulations:*

The tightness proof of the convex relaxation is analogous to the proof of adjacency of the segments in a piecewise linear (PWL) formulation. Ensuring the optimal solution abides by the adjacency conditions ensures that a PWL formulation can appropriately respond to an overload. In addition, augmenting the objective function with the temperature-underloading term presented in (3.54) will still preserve tightness since any optimal solution is incentivized to directly minimize $T[k]$ for k.